



HAL
open science

Effectiveness of a novel polyaniline@Fe-ZSM-5 hybrid composite for Orange G dye removal from aqueous media: Experimental study and advanced statistical physics insights

Abdelaziz Imgharn, Lahoucine Anchoum, Abdelghani Hsini, Yassine Naciri, Mohamed Laabd, Mohamed Mobarak, Nouh Aarab, Asmae Bouziani, Sabine Szunerits, Rabah Boukherroub, et al.

► To cite this version:

Abdelaziz Imgharn, Lahoucine Anchoum, Abdelghani Hsini, Yassine Naciri, Mohamed Laabd, et al.. Effectiveness of a novel polyaniline@Fe-ZSM-5 hybrid composite for Orange G dye removal from aqueous media: Experimental study and advanced statistical physics insights. *Chemosphere*, 2022, 295, pp.133786. 10.1016/j.chemosphere.2022.133786 . hal-03561674

HAL Id: hal-03561674

<https://hal.science/hal-03561674>

Submitted on 7 Nov 2022

HAL is a multi-disciplinary open access archive for the deposit and dissemination of scientific research documents, whether they are published or not. The documents may come from teaching and research institutions in France or abroad, or from public or private research centers.

L'archive ouverte pluridisciplinaire **HAL**, est destinée au dépôt et à la diffusion de documents scientifiques de niveau recherche, publiés ou non, émanant des établissements d'enseignement et de recherche français ou étrangers, des laboratoires publics ou privés.

Journal Pre-proof

Effectiveness of a novel polyaniline@Fe-ZSM-5 hybrid composite for Orange G dye removal from aqueous media: Experimental study and advanced statistical physics insights

Abdelaziz Imgharn, Lahoucine Anchoum, Abdelghani Hsini, Yassine Naciri, Mohamed Laabd, Mohamed Mobarak, Nouh Aarab, Asmae Bouziani, Sabine Szunerits, Rabah Boukherroub, Rajae Lakhmiri, Abdallah Albourine

PII: S0045-6535(22)00279-X

DOI: <https://doi.org/10.1016/j.chemosphere.2022.133786>

Reference: CHEM 133786

To appear in: *ECSN*

Received Date: 25 September 2021

Revised Date: 5 January 2022

Accepted Date: 27 January 2022

Please cite this article as: Imgharn, A., Anchoum, L., Hsini, A., Naciri, Y., Laabd, M., Mobarak, M., Aarab, N., Bouziani, A., Szunerits, S., Boukherroub, R., Lakhmiri, R., Albourine, A., Effectiveness of a novel polyaniline@Fe-ZSM-5 hybrid composite for Orange G dye removal from aqueous media: Experimental study and advanced statistical physics insights, *Chemosphere* (2022), doi: <https://doi.org/10.1016/j.chemosphere.2022.133786>.

This is a PDF file of an article that has undergone enhancements after acceptance, such as the addition of a cover page and metadata, and formatting for readability, but it is not yet the definitive version of record. This version will undergo additional copyediting, typesetting and review before it is published in its final form, but we are providing this version to give early visibility of the article. Please note that, during the production process, errors may be discovered which could affect the content, and all legal disclaimers that apply to the journal pertain.

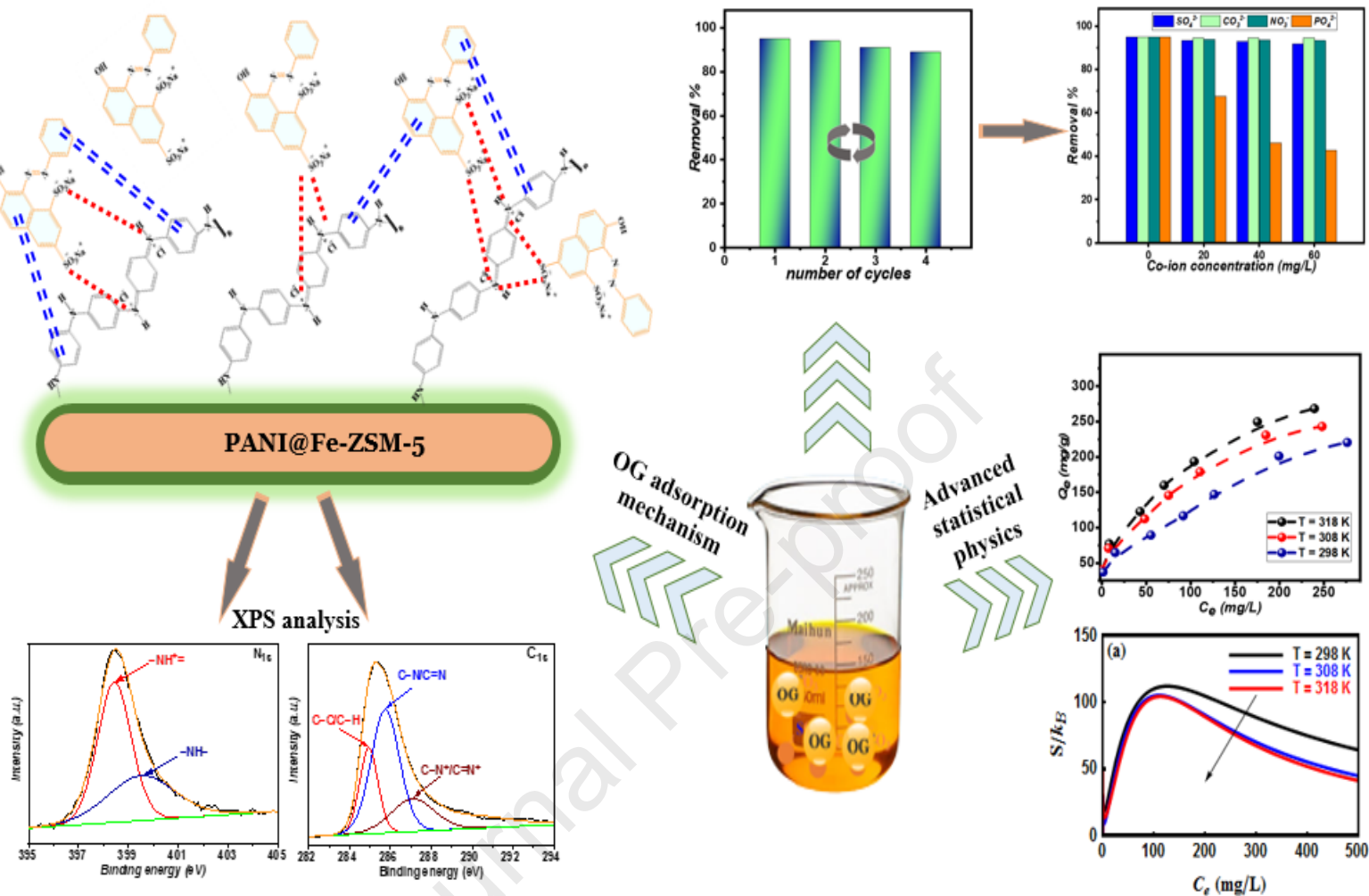
© 2022 Published by Elsevier Ltd.



Author Contributions Statement

Abdelaziz Imgharn: Formal analysis, Data curation, Writing-original draft. **Lahoucine Anchoum:** Investigation. **Abdelghani Hsini:** Methodology, Formal analysis, Data curation, Writing-review & editing. **Yassine Naciri:** Methodology, Investigation, Writing-review & editing. **Mohamed Laabd:** Validation, Writing-review & editing. **Mohamed Mobarak:** Formal analysis, Data curation. **Nouh Aarab:** Investigation. **Asmae Bouziani:** Writing-review & editing. **Sabine Szunerits:** Investigation, Methodology. **Rabah Boukherroub:** Conceptualization, Validation, Writing-review & editing. **Rajae Lakhmiri:** revision, editing. **Abdallah Albourine:** Conceptualization, Validation, revision, editing, Supervision, Project administration.

Graphical abstract



1 **Effectiveness of a novel polyaniline@Fe-ZSM-5 hybrid composite for Orange**
2 **G dye removal from aqueous media: Experimental study and advanced**
3 **statistical physics insights**

4 Abdelaziz Imgharn^{a, *}, Lahoucine Anouchm^a, Abdelghani Hsini^a, Yassine Naciri^a, Mohamed
5 Laabd^a, Mohamed Mobarak^b, Nouh Aarab^a, Asmae Bouziani^c, Sabine Szunerits^d, Rabah
6 Boukherroub^d, Rajae Lakhmiri^e, Abdallah Albourine^{a,*}

7 ^a*Laboratory of Materials and Environment, Faculty of Sciences, Ibn Zohr University, Agadir, Morocco.*

8 ^b*Physics Department, Faculty of Science, Beni-Suef University, Beni-Suef 62511, Egypt.*

9 ^c*Chemical Engineering Department, Middle East Technical University, Ankara, Turkey.*

10 ^d*Univ. Lille, CNRS, Centrale Lille, Univ. Polytechnique Hauts-de-France, UMR 8520 - IEMN, Lille F-*
11 *59000, France.*

12 ^e*Laboratory of Chemical Engineering and Valorization Resources, Faculty of Sciences and Techniques,*
13 *Abdelmalek Essaadi University, Tangier, Morocco.*

14 * Corresponding authors:

15 E-mail address: abdelaziz.imgharn@edu.uiz.ac.ma (A. Imgharn)

16 E-mail address: albourine@yahoo.fr (A. Albourine)

17

18

19

20

21

22

Abstract

A polyaniline@Fe-ZSM-5 composite was synthesized *via* an *in situ* interfacial polymerization procedure. The morphology, crystallinity, and structural features of the as-developed PANI@Fe-ZSM-5 composite were assessed using scanning electron microscopy – energy dispersive spectroscopy (SEM-EDS), X-ray diffraction (XRD), Fourier-transform infrared (FTIR) spectroscopy, and X-ray photoelectron spectroscopy (XPS). The composite was efficiently employed for the first time as an adsorbent to adsorb Orange G (OG) dyestuff from water. The OG dye adsorption performance was investigated as a function of several operating conditions. The kinetic study demonstrated that a pseudo-second-order model was appropriate to anticipate the OG adsorption process. The maximum adsorption capacity was found to be 217 mg/g. The adsorption equilibrium data at different temperatures were calculated *via* advanced statistical physics formalism. The entropy function indicated that the disorder of OG molecules improved at low concentrations and lessened at high concentrations. The free enthalpy and internal energy functions suggested that the OG adsorption was a spontaneous process and physisorption in nature. Regeneration investigation showed that the PANI@Fe-ZSM-5 could be effectively reused up to five cycles. The main results of this work provided a deep insight on the experimental study supported by advanced statistical physics prediction for the adsorption of Orange G dye onto the novel polyaniline@Fe-ZSM-5 hybrid composite. Additionally, the experimental and advanced statistical physics findings stated in this study may arouse research interest in the field of wastewater treatment.

Keywords: Polyaniline; Fe-ZSM-5; Composite; Dye removal; Advanced statistical physics; Regeneration.

46 **1. Introduction**

47 Many industries use synthetic dyes to color their final product, including food, drugs,
48 cosmetics, paper, leather, plastics, and textile (Abbasi, 2017). Dyes often exhibit
49 persistence to biodegradation and significant toxic, carcinogenic, and mutagenic effects
50 on aquatic organisms and humans, which has become a severe environmental problem in
51 the world (Belbachir and Makhoukhi, 2017; Gottlieb et al., 2003). Therefore, the discharge
52 of dyes in wastewater, even in a small amount, is unpleasant and should be removed
53 before they enter the environment. In this context, several treatment processes, including
54 coagulation-flocculation (Renault et al., 2009), photocatalysis (Akhsassi et al., 2021;
55 Fahoul et al., 2022; Mimouni et al., 2021; Naciri et al., 2021), ion exchange (Hassan and
56 Carr, 2018), membrane filtration, and adsorption (Amjlef et al., 2021; Imgharn et al.,
57 2021; Njoya et al., 2020) have been implemented to clean up colored effluents. Adsorption
58 is considered an effective, green, and low-cost approach used for dye elimination from
59 aqueous solutions. Therefore, the last decades have witnessed a huge interest in the
60 development of efficient adsorbent materials. The performance of adsorbents depends on
61 their physicochemical characteristics like porosity, particle size, surface functional groups,
62 and chemical stability (Benjelloun et al., 2021; Laabd et al., 2021).

63 π -Conjugated polymers including polyaniline (PANI), polythiophene (PTh), and
64 polypyrrole (PPy) have been widely employed in many fields like gas sensors, tissue
65 engineering, photovoltaic cells, batteries, and wastewater purification (Liao et al., 2019).
66 PANI is considered as the most promising conductive polymer among these polymers due
67 to its particular characteristics: good redox reversibility, low-cost, environmental
68 friendliness, excellent stability, good conductivity, and easy synthesis (Laabd et al., 2017;

69 Naciri et al., 2022). In addition, the uptake of organic dyes and heavy metal ions by PANI
70 is high. The ion exchange property, porous structure as well as the presence of a large
71 amount of protonated amine and imine groups on the surface of PANI are the reasons for
72 its high adsorption capacity. However, the small particle size and poor physical
73 (mechanical and thermal) properties of PANI seriously hinder its use in large scale
74 wastewater purification systems (Sahu et al., 2019). In order to counterbalance these
75 limitations, PANI-based composites using different reinforcing substrates like mineral
76 clays (Zhou et al., 2017), natural lignocellulosic wastes (Kumar et al., 2008), activated
77 carbon (Ansari et al., 2017) and zeolites (Abdellaoui et al., 2020; Shyaa et al., 2015) have
78 been developed.

79 Zeolite has a tridimensional form of crystalline aluminosilicate, an open anionic
80 framework consisting of tetrahedral oxygen-sharing TO_4 , in which AlO_4 and SiO_4 are
81 covalently linked to each other (Ba Mohammed et al., 2020; Shyaa et al., 2015). Besides,
82 the zeolitic materials are microporous with a uniform pore distribution. As evidenced from
83 the literature, the properties of zeolites can be enhanced by integrating different metals
84 into their matrices. Incorporation of iron into adsorbents is highly preferred due to its
85 economic, eco-friendly and semiconducting properties (Saifuddin et al., 2019). Several
86 works focused on the optimization of the adsorption parameters and discussed the
87 physical aspects of the process. However, only a restricted number of studies are available
88 which decipher the main role of the active metal ions of the zeolite structure in the
89 adsorption phenomenon.

90 Herein, we synthesized PANI@Fe-ZSM-5 zeolite hybrid composite through an oxidative
91 polymerization route and characterized by SEM coupled with EDS, XRD, FTIR and XPS

92 analysis. The initial Orange G (OG) concentration, dosage of adsorbent, contact time,
93 initial pH value of the solution and temperature were optimized to evaluate the
94 effectiveness of the synthesized PANI@Fe-ZSM-5 composite for OG removal. The
95 modeling of the equilibrium isotherms and adsorption kinetics of the OG dye on the
96 composite was also evaluated. Furthermore, the theoretical predication of the OG
97 molecules' binding on the surface of PANI@Fe-ZSM-5 was calculated using advanced
98 statistical physics applied to the adsorption equilibrium. In addition, the effect of co-
99 existing ions was assessed. Finally, the regeneration of PANI@Fe-ZSM-5 composite was
100 performed to evaluate its reusability for OG dyestuff removal.

101 **2. Experimental**

102 **2.1. Chemicals**

103 Aniline monomer (Sigma-Aldrich) was used after distillation. Sodium persulfate
104 ($\text{Na}_2\text{S}_2\text{O}_8$), acetone, ethanol, tetrapropylammonium bromide ($\text{C}_{12}\text{H}_{28}\text{NBr}$, 98 %), iron
105 (III) nitrate pentahydrate ($\text{Fe}(\text{NO}_3)_3 \cdot 5\text{H}_2\text{O}$, ≥ 99.95 %), sulfuric acid (H_2SO_4 , ≥ 95 %),
106 sodium metasilicate (Na_2SiO_3 , ≥ 98 %), hydrochloric acid (HCl, 37 %), sodium hydroxide
107 (NaOH, ≥ 97 %), sodium chloride (NaCl, ≥ 99 %), and orange G (OG) dye were of analytical
108 grade and purchased from Sigma-Aldrich. The dye solution was prepared by dissolving
109 the accurately weighted dye in distilled water.

110 **2.2. Preparation of Fe-ZSM-5 zeolite**

111 The Fe-ZSM-5 zeolite synthesis was conducted using the procedure reported by Ba
112 Mohammed et al. (Ba Mohammed et al., 2020). Briefly, 10 g of sodium metasilicate as a
113 silicon precursor were dissolved in 25 mL of distilled water, and then 2 g of
114 tetrapropylammonium bromide were added to the suspension under magnetic stirring

115 until the solution became uniform with a pH value of 10. The obtained solution was called
116 first solution. A second solution was produced by dissolving 1 g of ferric nitrate
117 pentahydrate in 10 mL of distilled water; then, the resulting solution was acidified using
118 2 ml of H₂SO₄ (0.01 M). This solution was poured dropwise into the first one and kept
119 under stirring for 2 h. The formed gel was placed in a Teflon autoclave at 180 °C for 48 h.
120 The resulting suspension was filtered and washed several times with acetone and distilled
121 water. Finally, the as-prepared material was kept at 100 °C overnight to dry then calcined
122 at 550 °C for 6 h.

123 **2.3. Elaboration of PANI@Fe-ZSM-5**

124 The PANI@Fe-ZSM-5 hybrid composite was prepared via an *in situ* oxidative
125 polymerization of aniline with Fe-ZSM-5 particles in an acidic medium using Na₂S₂O₈ as
126 oxidant, according to the procedure in (Hsini et al., 2021b): 1g of Fe-ZSM-5 was dispersed
127 in 100 mL of a hydrochloric acid solution (1M) under stirring for 6 h. Then, 0.5 mL of
128 aniline was added to the suspension under stirring for 3 h. A 50 mL solution of HCl (1 M)
129 containing sodium persulfate (with a 0.5 monomer/oxidant molar ratio) was added
130 dropwise into the mixture under agitation. A green suspension was obtained after 12 h,
131 indicating the formation of doped PANI on the Fe-ZSM-5 particles. The resulting
132 precipitate was filtered and washed with distilled water and acetone. The PANI@Fe-ZSM-
133 5 composite was dried at 70 °C overnight.

134 **2.4. Characterization of the adsorbent**

135 To check out the hybrid composite crystal structure, X-ray powder diffraction (XRD)
136 analyses were carried out with a BRUKER D8 ADVANCE TWIN diffractometer. The Fe-
137 ZSM-5 surface morphology before and after polymerization was systematically

138 characterized by scanning electron microscopy (SEM) coupled with energy dispersive X-
139 ray spectrometry (EDS) analysis (SEM, JEOL, JSM-IT200). X-ray photoelectron
140 spectroscopy (XPS) analysis of the as-prepared PANI@Fe-ZSM5 composite was acquired
141 using an ESCALAB 220 XL spectrometer equipped with a monochromatic Al K α X-ray
142 radiation source at 1486.6 eV. The binding energies were calibrated to the C1s peak at
143 284.6 eV. Fourier-transform infrared (FTIR) spectra of the obtained materials were
144 acquired using KBr pellets using FTIR spectroscopy (ALPHA-Bruker Optics, Germany) in
145 a wavenumber ranging from 400 to 4000 cm⁻¹.

146 The zero charge point (PZC) of the PANI@Fe-ZSM-5 composite was determined via
147 potentiometric titration method reported by Fiol and Villaescusa (Fiol and Villaescusa,
148 2009). In short, 0.025 g of PANI@Fe-ZSM-5 was added to 50 mL of KNO₃ (0.03 M)
149 solution and the pH of the solution was adjusted from 2 to 12 by adding HCl (0.1 M) or
150 NaOH (0.1 M) aqueous solutions. The mixtures were stirred for 24 h at ambient
151 temperature. The final pH_f of each solution was assessed. Then, the PZC was identified as
152 pH_i when ΔpH is zero.

153 **2.5. Adsorption experiments and regeneration**

154 The OG dye adsorption onto PANI@Fe-ZSM-5 hybrid composite was conducted in a batch
155 reactor under various operational conditions. To evaluate the effect of adsorbent dose,
156 various amounts of PANI@Fe-ZSM-5 composite (0.2-2 g/L) were introduced into 50 mL
157 of OG dye solution at 20 mg/L initial concentration for 180 min at pH 6.0 and 25 °C. The
158 influence of pH on the OG dye removal efficiency was studied by changing the solution pH
159 from 2 to 12 with an adsorbent dose of 0.5 g/L. Under the same experimental conditions,
160 the influence of initial concentration of OG dye (from 20 to 500 mg/L), contact time and

161 temperature was also assessed. After adsorption, the adsorbent was removed from
162 adsorbate solution by filtration on Millipore filters (0.45 μm). The equilibrium
163 concentration of OG dye was quantified by UV2300 spectrophotometer at 476 nm.

164 The **absorbed** percentage $R(\%)$ and the adsorption capacity $Q_e(\text{mg/g})$ were calculated by
165 the following relations (Ait Haki et al., 2021; Brini et al., 2021b):

$$166 \quad R\% = \frac{(C_0 - C_e)}{C_0} \times 100 \quad (1)$$

$$167 \quad Q_e = \frac{(C_0 - C_e) \cdot V}{m} \quad (2)$$

168 Where C_0 (mg/L) is the initial OG concentration, C_e (mg/L) is the OG concentration at
169 equilibrium, m (g) is the mass of the PANI@Fe-ZSM-5 composite, and V (L) is the volume
170 of the solution.

171 In order to bring up the adsorption process more economically reliable and eco-friendly,
172 the regeneration of PANI@Fe-ZSM-5 composite after the adsorption experiment is a very
173 important aspect. For desorption/adsorption study, 0.3 g of PANI@Fe-ZSM-5 was
174 introduced in 0.6 L of 20 mg/L OG dye solution. After 180 min of sorption, desorption
175 experiment was performed using 0.5 M NaOH as eluent solution for 6 h. After that, the
176 regenerated PANI@Fe-ZSM-5 composite was washed with distilled water, and then
177 redoped with 1 M HCl solution. The fresh PANI@Fe-ZSM-5 composite was used for a
178 subsequent OG adsorption cycle. In this work, five regeneration cycles were carried out.

179 **2.6. Theoretical background**

180 The statistical physics theory is an emerging effective approach to deeply illuminate the
181 adsorption mechanisms at the liquid-solid interface (Mobarak et al., 2019b, 2019a;

182 Mohamed et al., 2020). The adsorption performance of OG dye on the PANI@Fe-ZSM-5
 183 hybrid composite was examined by applying five statistical physics models to the
 184 experimental equilibrium data.

185 ○ First model (**M1**): Monolayer model with similar receptor sites. This model assumes
 186 that the adsorption process occurs by the formation of a monolayer on the adsorbent
 187 surface with one type of adsorption sites (Mobarak et al., 2019b, 2019a). The
 188 analytical expression of the M1 model is given by Eq. (3):

$$189 \quad Q_e = nN_o = \frac{nN_M}{1 + \left(\frac{C_{1/2}}{C_e}\right)^n} = \frac{Q_{sat}}{1 + \left(\frac{C_{1/2}}{C_e}\right)^n} \quad (3)$$

190 where Q_e (mg/g) and C_e (mg/L) denote the equilibrium adsorbed amount and equilibrium
 191 concentration, respectively; n represents the number of adsorbed molecules per binding
 192 site; N_M (mg/g) is the active sites density; Q_{sat} (mg/g) is the adsorption capacity at
 193 saturation; $C_{1/2}$ (mg/L) is the adsorbate concentration at half-saturation.

194 ○ Second model (**M2**): Double-layer model with similar receptor sites. This model is
 195 appropriate to describe the double-layer adsorption process over the adsorbent surface
 196 with identical binding sites. The formalism of the M2 model is presented by Eq. (4):

$$197 \quad Q_e = nN_M \frac{\left(\frac{C_e}{C_{1/2}}\right)^n + 2\left(\frac{C_e}{C_{1/2}}\right)^{2n}}{1 + \left(\frac{C_e}{C_{1/2}}\right)^n + \left(\frac{C_e}{C_{1/2}}\right)^{2n}} \quad (4)$$

198 ○ Third model (**M3**): Monolayer model with two different energies. This model is
 199 established on the hypothesis that the adsorption process is a monolayer coverage over
 200 two kinds of adsorbent active sites (with different energies) (Mobarak et al., 2019b,
 201 2019a).

$$202 \quad Q_e = \frac{n_1 N_{1M}}{1+(C_1/C_e)^{n_1}} + \frac{n_2 N_{2M}}{1+(C_2/C_e)^{n_2}} \quad (5)$$

203 where C_1 and C_2 (mg/L) are the half-saturation concentrations for the first and the second
 204 adsorption sites, respectively; N_{1M} and N_{2M} (mg/g) are the receptor site densities of the
 205 first and the second kinds of active sites, respectively; n_1 and n_2 are the number of
 206 adsorbed molecules by each binding site for the first and the second kinds of active sites,
 207 respectively.

208 ○ Fourth model (**M4**): Double-layer model with two different energies. This model is
 209 suitable to predict the double-layer adsorption on the two different types of adsorbent
 210 active sites. The equation of the M4 model is given as:

$$211 \quad Q_e = nN_M \frac{\left(\frac{C}{C_1}\right)^n + 2\left(\frac{C}{C_2}\right)^{2n}}{1 + \left(\frac{C}{C_1}\right)^n + \left(\frac{C}{C_2}\right)^{2n}} \quad (6)$$

212 where C (mg/L) denotes the equilibrium concentration; N_M (mg/g) refers to receptor
 213 sites density; C_1 and C_2 (mg/L) correspond to the concentrations at half-saturation for
 214 the first and the second type of active sites, respectively.

215 ○ Fifth model (**M5**): Finite multi-layer model. This model suggests the occurrence of
 216 multilayer adsorption process. The formalism of the M5 model is expressed as follows:

$$217 \quad Q_e = nN_M \frac{\left(\frac{C}{C_1}\right)^n \left(1 - (N_\ell + 1) \left[\frac{C}{C_2}\right]^{nN_\ell} + N_\ell \left[\frac{C}{C_2}\right]^{n(N_\ell + 1)}\right)}{\left(1 - \left[\frac{C}{C_2}\right]^n\right) \left(1 - \left[\frac{C}{C_2}\right]^n + \left[\frac{C}{C_1}\right]^n - \left[\frac{C}{C_1}\right]^n \left[\frac{C}{C_2}\right]^{nN_\ell}\right)} \quad (7)$$

218 where $(N_\ell + 1)$ represents the number of adsorption layers; n refers to the number of
 219 ions per adsorption site; N_M (mg/g) refers to receptor sites density; C_1 and C_2 (mg/L)

220 correspond to the concentrations at half-saturation for the first and the second type of
 221 active sites, respectively.

222 The equations of the above-presented statistical physics models were derived from the
 223 corresponding grand-canonical partition functions in the statistical physics (Mobarak et
 224 al., 2019b, 2019a). These models were fitted to the experimental results of OG dye
 225 adsorption onto PANI@Fe-ZSM-5 composite using Mathematica 11 program. The
 226 appropriateness of the selected models was evaluated based on the correlation coefficient
 227 (R^2) and root mean squared error (RMSE) values (Mobarak et al., 2019b).

$$228 \quad RMSE = \sqrt{\frac{\sum_{i=1}^m (Q_{i\text{ cal}} - Q_{i\text{ exp}})^2}{p - q}} \quad (8)$$

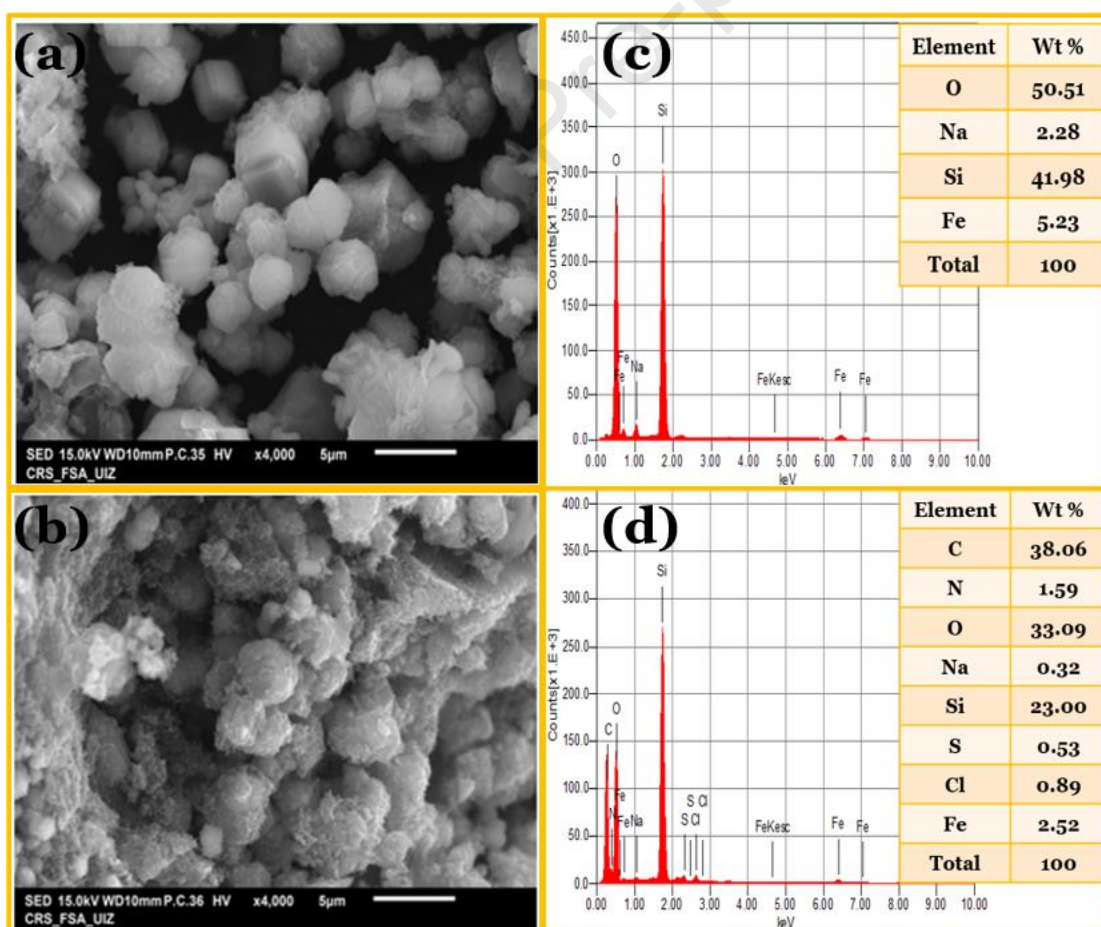
229 where p and q represent the number of actual data and adjustable parameters,
 230 respectively. $Q_{i\text{ cal}}$ and $Q_{i\text{ exp}}$ denote the computed and the experimental OG dye uptake
 231 capacities, respectively.

232 **3. Results and discussion**

233 **3.1. Surface characterization and XRD analysis**

234 **Fig. 1** depicts the morphology and elemental analysis of Fe-ZSM-5 particles before and
 235 after the polymerization of aniline. According to **Fig. 1(a)**, the SEM image of Fe-ZSM-5
 236 features smooth agglomerated spheres with a size ranging from 1 to 5 μm . **Fig. 1(b)**
 237 confirms the deposition of polyaniline onto the Fe-ZSM-5 surface with a flake-like
 238 structure. This surface morphology may constitute a good platform for the removal of
 239 pollutants from aqueous media. In addition, the acquired textural information reveals
 240 good adhesion of PANI onto the Fe-ZSM-5 surface. This may be due to interactions

241 (hydrogen bonds) between the amine groups of aniline and the hydroxyl groups (Si-OH)
 242 of the Fe-ZSM-5 zeolite (Ba Mohammed et al., 2020). From **Figs. 1(c)** and **(d)**, the
 243 elemental analysis of the Fe-ZSM-5 zeolite by EDS proves the existence of the following
 244 elements: oxygen (50.51%), silicon (41.98%), iron (5.23%) and sodium (2.28%). This
 245 result indicates that silicon oxide (SiO₂) is the major phase of the Fe-ZSM-5 zeolite. After
 246 the polymerization of aniline on the surface of Fe-ZSM-5 zeolite, the EDS spectrum shows
 247 the appearance of carbon (38.06%). In addition, the EDS spectrum of PANI@Fe-ZSM-5
 248 features other characteristic elements (N, Cl and S), which affirms that the surface of Fe-
 249 ZSM-5 is well-coated by PANI.



250

251 **Fig. 1. (a)** SEM micrographs of Fe-ZSM-5, **(b)** PANI@Fe-ZSM-5 and **(c and d)** their
252 respective EDS elemental spectra.

253 X-ray diffraction is an important technique used to identify the crystalline phases and
254 structural properties of solid materials. Therefore, the as-prepared Fe-ZSM-5 zeolite and
255 PANI@Fe-ZSM-5 composite were analyzed by this technique and the obtained XRD
256 patterns are displayed in **Fig. 2(a)**. The synthesized Fe-ZSM-5 zeolite sample exhibited
257 peaks at $2\theta=7.95^\circ$, 8.80° , 23.10° , 23.94° and 24.40° associated with [0 1 1], [0 2 0], [0 5
258 1], [0 3 3] and [3 1 3] planes, with corresponding d-spacing values of 1.11, 1.00, 0.38, 0.37
259 and 0.36 nm, respectively. These values are in good agreement with the peaks of Fe-ZSM-
260 5 zeolite (JCPDS no. 43-0321) with a well-resolved mordenite framework inverted (MFI)
261 structure (Chemical formula: $H_{0.32}Al_{0.32}Si_{95.68}O_{192}$, Crystal system: Monoclinic and Space
262 group: P21/n) (Narayanan et al., 2015). Moreover, the sharpness of the peaks of the
263 diffraction peaks suggests that the as-prepared Fe-ZSM-5 sample has a more crystalline
264 nature and no other peaks appeared, which discloses that the as-prepared Fe-ZSM-5
265 material does not contain any impurities (Liu et al., 2011). Compared with bare Fe-ZSM-
266 5 sample, the peak intensities of the [0 1 1] and [0 2 0] planes of PANI@Fe-ZSM-5
267 composite were markedly decreased due to the PANI coating on the Fe-ZSM-5 surface,
268 but their crystal framework structure was preserved. Moreover, no characteristic
269 diffraction peaks of PANI were detected in PANI@ZSM-5 composite, because PANI was
270 in amorphous phase. Furthermore, the absence of impurity phases in the XRD curves
271 indicates the successful synthesis of PANI@Fe-ZSM-5 composite.

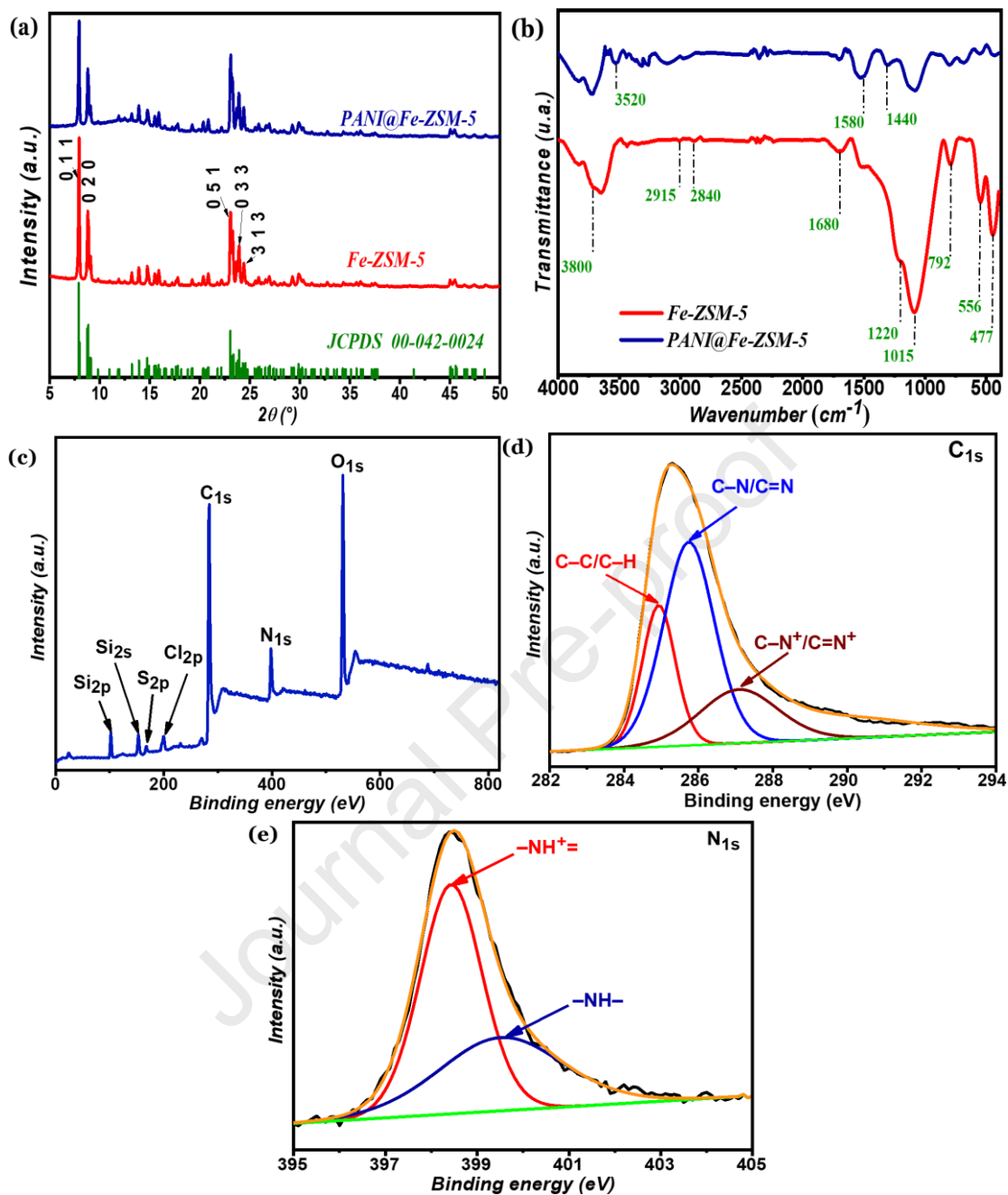
272 **3.2. FTIR data analysis**

273 The FTIR spectrum of Fe-ZSM-5 and PANI@Fe-ZSM-5 are depicted in **Fig. 2(b)**. The
274 FTIR spectrum of Fe-ZSM-5 exhibits a characteristic peak at about 3854 cm^{-1} ascribed to
275 the silanol groups of Si-OH. The absorption bands at 2915 and 2840 cm^{-1} can be assigned
276 to the residual methyl ($-\text{CH}_3$) and methylene ($-\text{CH}_2$) vibrations of tetrapropylammonium
277 bromide precursor (Kachangoon et al., 2020). The peak located at 1631 cm^{-1} is ascribed
278 to the stretching bending of adsorbed water molecules. The symmetric stretching of
279 external linkages of the tetrahedron appears at around 792 cm^{-1} (Liu et al., 2011). Also,
280 the spectrum comprises a peak at 556 cm^{-1} assigned to the stretching vibrations of Fe-O
281 of Fe_2O_3 (Suresh et al., 2014). The peaks at 477 and 1220 cm^{-1} are attributed to the Si-O
282 bending vibrations of SiO_4 internal tetrahedral (Doula, 2007), (Niu et al., 2017). The FTIR
283 spectrum of PANI@Fe-ZSM-5 reveals the appearance of a new peak at 3520 cm^{-1} assigned
284 to the N-H stretching vibration, indicating the existence of amine groups. Besides, the
285 vibration bands at 1580 and 1440 cm^{-1} are ascribed to the stretching vibration C=C in
286 quinoid and benzenoid structure of doped PANI, respectively (Xu et al., 2014). These
287 findings confirm that the PANI was well-incorporated onto the surface of Fe-ZSM-5
288 particles.

289 **3.3. XPS analysis**

290 XPS analysis was performed to assess the chemical composition and chemical state of the
291 PANI@Fe-ZSM5 surface. The full survey XPS survey of PANI@Fe-ZSM5 composite is
292 depicted in **Fig. 2(c)**. The spectrum revealed the presence of O_{1s} (531.5 eV), N_{1s} (397.9 eV)
293 and C_{1s} (283.6 eV) as the main components of the PANI@Fe-ZSM5 surface (Abdel Hamid
294 et al., 2019). Besides, the presence of three weak peaks confirmed the occurrence of silicon
295 (Si_{2p} and Si_{2s} at 101.9 and 152.6 eV , respectively), sulfur (S_{2p} at 168.1 eV) and chlorine

296 (Cl_{2p} at 199.4 eV) elements on the PANI@Fe-ZSM-5 surface (Abdel Hamid et al., 2019;
297 Ravelo-Acuña et al., 2019; Zhang et al., 2016). The Si element is related to the silica in the
298 ZSM-5 zeolite. The other elements (e.g., Fe and Al) of Fe-ZSM-5 zeolite were not detected,
299 which eventually due to the formation of thick PANI layer on the surface of Fe-ZSM-5
300 zeolite (penetration depth of the X-ray beam does not exceed 10 nm). The Cl and S
301 elements are indicative of the existence of chloride anion doping (Cl⁻) and oxidizing agent
302 (sodium persulfate) on the PANI@Fe-ZSM-5 surface. From **Fig. 2(d)**, the C_{1s} high
303 resolution spectrum was fitted with three peaks located at 284.9 (C–C/C–H), 285.7 (C–
304 N/C=N) and 287.1 eV (C–N⁺/C=N⁺) (Chan et al., 1992; Wang et al., 2015). The positively
305 charged N-containing functional groups indicated the doping of PANI chains by sulfate
306 and chloride ions generated from the oxidant and HCl acid (Wang et al., 2005). **Fig. 2(e)**
307 shows that the N_{1s} spectrum which can be deconvoluted into two peaks at 398.4 and 399.6
308 eV ascribed to amine (–NH–) and doped quinonoid imine (–NH⁺⁼) of benzenoid ring,
309 respectively (Bhaumik et al., 2021). The XPS results demonstrated that the PANI
310 Emeraldine salt (doped form) was successfully coated on the Fe-ZSM-5 zeolite.



311

312 **Fig.2. (a)** XRD patterns of Fe-ZSM-5 and PANI@Fe-ZSM-5 composite; **(b)** FTIR313 spectra of Fe-ZSM-5 zeolite and PANI@Fe-ZSM-5 composite; **(c)** XPS wide scan314 spectrum; **(d)** C_{1s} and **(e)** N_{1s} core level spectra of the PANI@Fe-ZSM-5 composite.

315

3.4. Adsorption study

3.4.1. Effects of adsorbent dosage and pH

The influence of sorbent dosage on the OG dye adsorption was investigated in the 0.2 to 2.0 g/L concentration range. **Fig. 3(a)** displays the removal efficiency and uptake capacity of OG onto PANI@Fe-ZSM-5 at different adsorbent doses. The adsorption percentage was increased up to 96.37 % with the increase of PANI@Fe-ZSM-5 dose from 0.2 to 0.5 g/L. This might be due to the increment in the number of adsorbate binding sites available for OG dye removing (Hsini et al., 2020). Increasing the PANI@Fe-ZSM-5 dosage beyond 0.5 g/L did not affect the OG dye adsorption efficiency. This trend may be due to the exhaustion of OG dye molecules. Besides, the uptake capacity was decreased, owing to the formation of adsorbent particles aggregates, which could minimize the availability of surface sites for OG dye adsorption (Hsini et al., 2021d; Tu et al., 2020).

It is widely-known that the solution pH is a key operating condition in adsorption processes (Hsini et al., 2021a). The surface charge of the PANI@Fe-ZSM-5 composite was investigated as a function of pH (inset of **Fig. 3(b)**). The PZC value of PANI@Fe-ZSM-5 composite was found to be 3.75. This means that the as-prepared PANI@Fe-ZSM-5 material surface is positively charged at pH below 3.75, while the surface becomes negatively charged at pH above 3.75. The influence of the solution pH on the adsorption process over the pH range 2–12 is displayed in **Fig. 3(b)**. As a result, the maximum removal percentage of OG dye was achieved at low pH values. That could be elucidated by the protonation of adsorbent sites (protonated silanol and amine groups), which results in the increment of the electrostatic interactions between anionic OG dye and positively charged PANI@Fe-ZSM-5 surface (Ba Mohammed et al., 2020). Whilst, at higher pH, the

339 OG dye adsorption efficiency decreased due to a decline of the number of positively
340 charged sites. Therefore, we can conclude that the adsorption of OG dye on the as-
341 prepared adsorbent surface is executed through electrostatic interactions (Yeamin et al.,
342 2021), as well as the involvement of π - π ones (Nasar and Mashkoor, 2019). Besides, under
343 alkaline conditions, the competitive adsorption of OH^- ions with OG anions could be
344 another reason to explain the observed downward trend of OG dye removal efficiency. In
345 the next adsorption experiments, the pH value of OG solutions was maintained at 6.0 to
346 minimize the costs related to the pH adjustment. It is worth highlighting the pivotal role
347 of electrostatic and π - π interactions in the OG dye adsorption mechanism. Based on the
348 above discussion, a binding mechanism of OG dye on the PANI@Fe-ZSM-5 surface is
349 proposed in **Fig. 6(d)**. To further confirm the adsorption of OG dye, the adsorbent surface
350 after adsorption was analyzed by the FTIR technique. The FTIR spectra of PANI@Fe-
351 ZSM-5 before and after OG dye removal are depicted in **Fig. 6(c)**. As a result, the FTIR
352 data showed that there is no obvious shift in the bands of the functional groups on the
353 PANI@Fe-ZSM-5 surface after adsorption, indicating that the molecular structure of the
354 PANI@Fe-ZSM-5 composite remained unaltered after OG dye removal. Furthermore,
355 no new peak was observed after OG adsorption, suggesting that there is no chemical
356 interaction of OG molecules with PANI@Fe-ZSM-5. Therefore, it can be concluded that
357 the binding of OG dye molecule on the PANI@Fe-ZSM-5 surface sites takes place via
358 physical interactions (e.g., electrostatic forces and π - π interactions). In light of the above
359 presented discussion, a graphical illustration of the proposed adsorption mechanism is
360 presented in **Fig. 6(d)**.

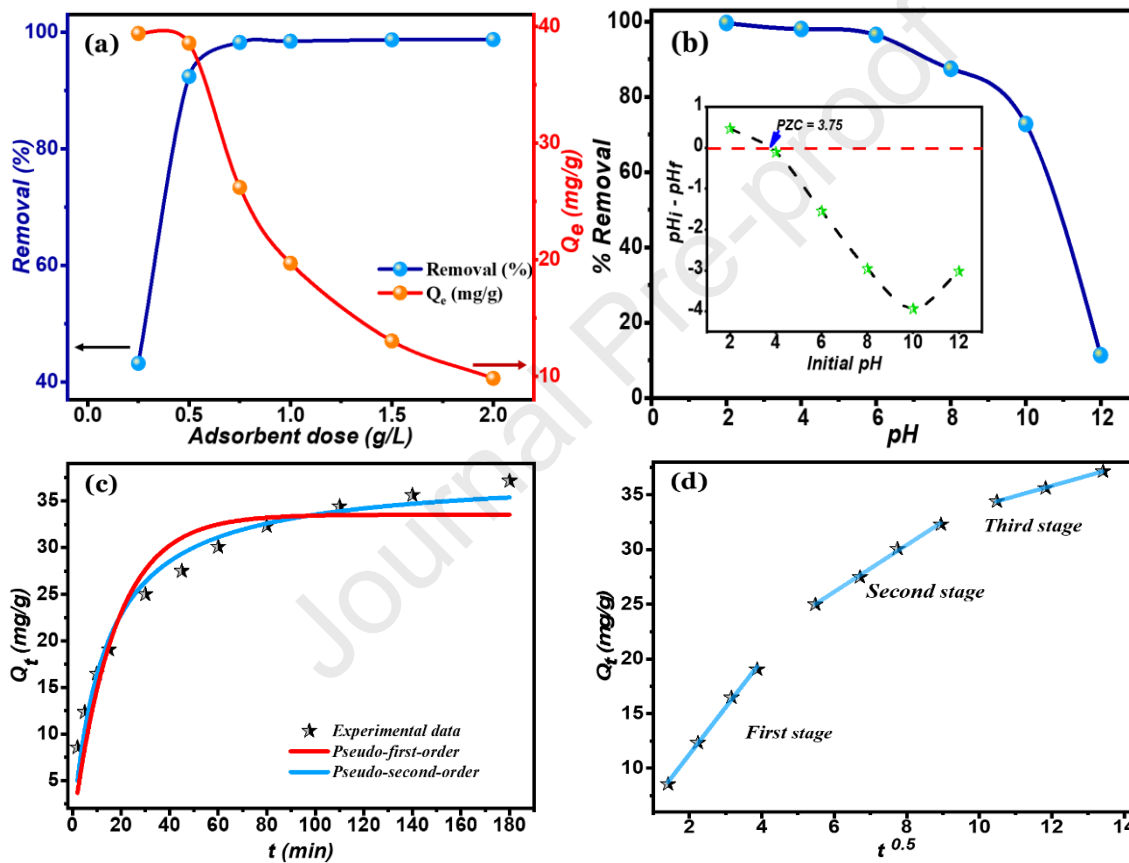
361

3.4.2. Adsorption kinetics

The result of adsorbent/adsorbate contact time on the removal of OG dye by PANI@Fe-ZSM-5 composite surface was investigated by plotting the adsorption capacity of OG dye versus contact time (from 2 to 180 min). The adsorbent dosage of 0.5 g/L was used in 100 mL of OG solution with 20 mg/L initial concentration at pH 6 and 25 °C. From **Fig. 3(c)**, it can be seen that upon increasing the contact time, the OG dye uptake was improved. In the first 60 min, the increase was rapid then it became slow, and the equilibrium was reached after 120 min. Thus, the removal ability of PANI@Fe-ZSM-5 composite was related to the binding sites availability on the PANI@Fe-ZSM-5 surface for OG textile dye removal (Tu et al., 2020). The pseudo-first-order, pseudo-second-order, and intraparticle diffusion kinetic models were used to fit the kinetic data to evaluate the kinetic mechanism of OG adsorption on the PANI@Fe-ZSM-5 composite (Abbasi, 2017). The nonlinear equations and the corresponding fitting parameters of pseudo-first-order and pseudo-second-order kinetic models are summated in **Table S1** and **Fig. 3(c)**. As shown in **Fig. 3(c)**, the pseudo-second-order model with R^2 of 0.97 is the model which had the highest correlation coefficient than the pseudo-first-order model (0.91). Furthermore, the adsorption capacity, calculated from pseudo-second-order model (37.99 mg/g), was found to be close to the experimentally-determined one (37.15 mg/g), confirming that the OG dye adsorption process was better described by this kinetic model.

In order to investigate the mass transfer mechanism that occurred during the adsorption process, the intraparticle diffusion model was applied to the actual removal data (Tang and Zhang, 2016). The fitting parameters are listed in **Table S1**. **Fig. 3(d)** illustrated that the removal of OG dye by the PANI@Fe-ZSM-5 composite consisted in three successive

385 stages. The first one was ascribed to the diffusion of OG dye molecules from the aqueous
 386 phase to the external surface sites of as-prepared composite. The second stage implicates
 387 the intra-particle diffusion as rate-controlling step. In the last stage the intraparticle
 388 diffusion rate decreased, because of the extremely low concentration of OG (Tang and
 389 Zhang, 2016). Besides, these results were supported by the reduction of rate constant
 390 values when going from the first stage to the last one.



398 **Fig. 3. (a)** Effect of PANI@Fe-ZSM-5 dose on the OG dye adsorption efficiency

399 (Conditions: equilibrium time = 180 min; OG dye concentration = 20 mg/L;

400 temperature = 25 °C); **(b)** Adsorption efficiency of the OG dye onto PANI@Fe-ZSM-5 at
 401 different pH values (inset: PZC determination of the PANI@Fe-ZSM-5 composite), **(c)**

402 Pseudo-first-order and pseudo-second-order kinetics models; **(d)** intraparticle diffusion

403 model.

404

405 **3.5. Advanced statistical physics interpretation**

406 The fitting of the considered statistical physics models to the experimental data for OG
407 dye removal by the PANI@Fe-ZSM-5 composite was evaluated based on the
408 determination of R^2 coefficient and RMSE values. From **Table S2**, it is clear that the **M3**
409 model (monolayer model with two different energies) demonstrated good correlation with
410 OG dye adsorption data (high R^2 values and low RMSE values) for all tested temperatures
411 (**Fig. 4(a)**). Therefore, the **M3** model was chosen as the best fitting statistical physics
412 model to elucidate the macroscopic and microscopic properties of the OG dye removal
413 process by the PANI@Fe-ZSM-5 composite.

414 **3.5.1. Statistical physics parameters**

415 To shed light on the orientation of OG dye molecules on the PANI@Fe-ZSM-5 surface, the
416 values of the stoichiometric coefficient (n) were calculated at different temperatures (**Fig.**
417 **4(b) and Table S3**). On the one hand, n_1 values (for the first type of active sites) are less
418 than 1, indicating that the OG dye molecules adsorbed parallelly on the first type of active
419 surface sites of PANI@Fe-ZSM-5 composite. In addition, each receptor site (first type) of
420 PANI@Fe-ZSM-5 composite adsorbs more than one OG dye molecule, suggesting a multi-
421 docking adsorption mechanism (Sellaoui et al., 2015). This adsorption behavior becomes
422 more pronounced with increasing temperature (n_1 values decreased). On the other hand,
423 the n_2 values (for the second type of active sites) are superior to unity, revealing that the
424 OG dye molecules adsorbed perpendicularly *via* a multimolecular mechanism on the
425 second type of active sites of PANI@Fe-ZSM-5 composite (Laabd et al., 2022). Moreover,
426 it is worth noticing that the n_2 values increased with the increase of temperature,

427 highlighting that the thermal agitation results in the decrease in the aggregation of the OG
428 dye molecules in the liquid phase (Li et al., 2019).

429 The density of active sites (N_M) is a crucial parameter governing the removal performance.
430 The temperature dependence of N_M parameter for OG dye removal by PANI@Fe-ZSM-5
431 composite surface is presented in **Fig. 4(c)**. It can be observed that the N_{1M} (for the first
432 type of active sites) and N_{2M} (for the second type of active sites) parameters follow an
433 inverse trend compared to n_1 and n_2 stoichiometric coefficients, respectively. This result
434 could be attributed to steric-hindrance effect of OG dye molecules during the adsorption
435 process onto the PANI@Fe-ZSM-5 surface (Sellaoui et al., 2017b). Indeed, as the number
436 of adsorbed OG dye molecules per active site (n) decreases, the number of available
437 adsorption sites increases, thus leading to an increase in the density of active sites (N_M),
438 and vice versa.

439 The saturation uptake capacity (Q_{sat} in mg/g) of the PANI@Fe-ZSM-5 composite for OG
440 dye adsorption depends on the stoichiometric coefficient (n) and density of active sites
441 ($Q_{\text{sat}} = nN_M$). From **Fig. 4(d)**, it is convenient to mention that the adsorbed amounts (Q_1
442 and Q_2) increased with raising the temperature (endothermic process), confirming that
443 the total OG dye adsorption capacity (Q_{sat}) is predominantly affected by the density of
444 active sites (N_M) rather than the stoichiometric coefficient (n).

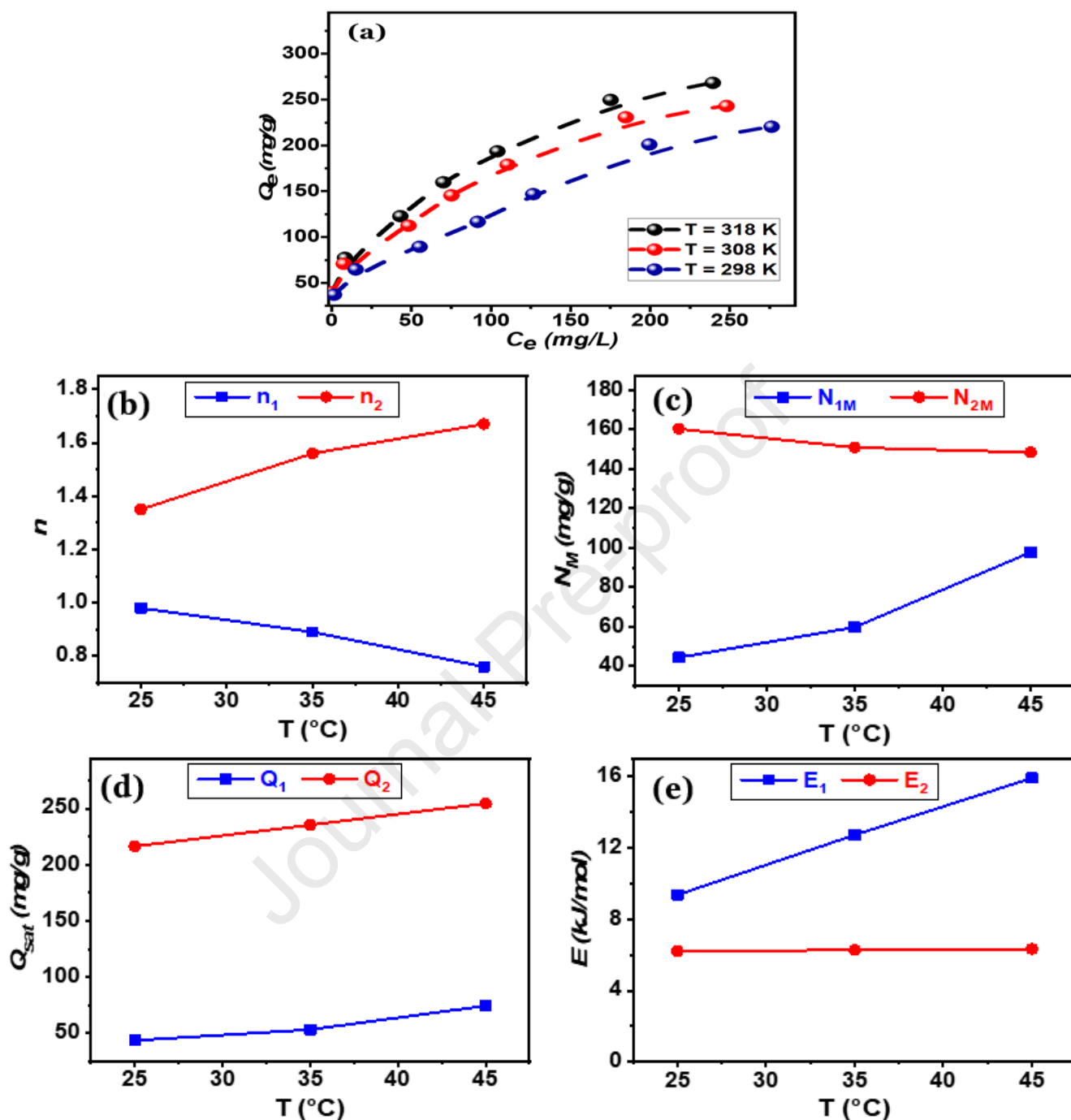
445 From an energetic point of view, the removal of OG dye by the PANI@Fe-ZSM-5
446 composite was assessed by calculating the adsorption energies E_1 and E_2 for the first and
447 second types of active sites, respectively. The values of E_1 and E_2 can be computed by the
448 following Eqs.:

$$449 \quad E_1 = RT \ln \left(\frac{C_s}{C_1} \right) \quad (9)$$

$$450 \quad E_2 = RT \ln \left(\frac{C_s}{C_2} \right) \quad (10)$$

451 where C_s (mg/L) is the aqueous solubility of OG dye. C_1 and C_2 represent the half-
452 saturation concentrations (mg/L) for the first and the second types of adsorption sites,
453 respectively. R (8.314 J/mol K) is the universal gas constant and T is the temperature (K).

454 **Fig. 4(e)** shows the influence of temperature on the removal energy. It is noteworthy
455 that the values of adsorption energies are positive and increased with temperature,
456 proving that the OG dye removal by the PANI@Fe-ZSM-5 composite is an endothermic
457 process. Therefore, the adsorption method is favorable at higher temperatures, which
458 is in concordance with the saturation adsorption capacity. Moreover, the figure shows
459 that E_1 is higher than E_2 , which **confirm** that PANI@Fe-ZSM-5 has a higher
460 interaction with OG dye. From the calculated values of adsorption energies, we deduce
461 that the adsorption was a physical process since these values are <40 kJ/mol (Seliem
462 and Mobarak, 2019). The adsorption **formed bonds could be a** hydrogen bonds or **Van**
463 **der Waals** or dipole-dipole interactions (Wjihi et al., 2020, 2017), reinforcing that the
464 OG dye adsorption is physisorption in nature (Sellaoui et al., 2016).



466 **Fig. 4. (a)** Fitting of actual equilibrium data of OG dye removal by the PANI@Fe-ZSM-5
 467 composite to the M3 model (best fitted model); **(b)** The stoichiometric coefficient; **(c)**
 468 the density of active sites; **(d)** the saturation uptake capacity and **(e)** the adsorption
 469 energy for OG dye removal by the PANI@Fe-ZSM-5 composite at different
 470 temperatures.

471 **3.5.2. Thermodynamic functions**

472 The thermodynamic functions (entropy, free enthalpy and internal energy) related to the
 473 OG dye adsorption on the PANI@Fe-ZSM-5 composite were calculated using the
 474 monolayer **layer** model with the different energy sites (**M3**). The entropy function is of
 475 prime importance to predict the randomness of OG dye molecules at the solution-
 476 adsorbent interface. This thermodynamic function was calculated according to the
 477 following Eq. (Seliem and Mobarak, 2019):

$$478 \frac{S}{k_B} = \frac{-Q_{sat.1} \left[\frac{c}{c_1} \right]^{n_1} \ln \left[\frac{c}{c_1} \right] + Q_{sat.2} \left[\frac{c}{c_2} \right]^{n_2} \ln \left[\frac{c}{c_2} \right] + \left[\frac{c}{c_1} \right]^{n_1} \left[\frac{c}{c_2} \right]^{n_2} (Q_{sat.1} \ln \left[\frac{c}{c_1} \right] + Q_{sat.2} \ln \left[\frac{c}{c_2} \right])}{\left(1 + \left[\frac{c}{c_1} \right]^{n_1} \right) \left(1 + \left[\frac{c}{c_2} \right]^{n_2} \right) + \ln \left(\left(1 + \left[\frac{c}{c_1} \right]^{n_1} \right)^{N_{1M}} \left(1 + \left[\frac{c}{c_2} \right]^{n_2} \right)^{N_{2M}} \right)} \quad (11)$$

479 To evaluate the spontaneity of the OG dye adsorption system, the free enthalpy function
 480 is computed as follows (Ayachi et al., 2019):

$$481 \frac{G}{k_B T} = \ln \left[\frac{\mu}{Z_{tr}} \right] \left(\frac{Q_{sat.1}}{1 + \left[\frac{c_1}{c} \right]^{n_1}} + \frac{Q_{sat.2}}{1 + \left[\frac{c_2}{c} \right]^{n_2}} \right) \quad (12)$$

482 The internal energy (E_{int}) represents the sum of energies in the adsorption system. This
 483 thermodynamic function is written as follows (Seliem and Mobarak, 2019):

$$484 \frac{E_{int}}{k_B T} = \frac{-N_{1M} \left[\frac{c}{c_1} \right]^{n_1} (n_1 \ln \left[\frac{c}{c_1} \right] - \mu) + N_{2M} \left[\frac{c}{c_2} \right]^{n_2} (n_2 \ln \left[\frac{c}{c_2} \right] - \mu) + \left[\frac{c}{c_1} \right]^{n_1} \left[\frac{c}{c_2} \right]^{n_2} (N_{1M} (n_1 \ln \left[\frac{c}{c_1} \right] - \mu) + N_{2M} (n_2 \ln \left[\frac{c}{c_2} \right] - \mu))}{\left(1 + \left[\frac{c}{c_1} \right]^{n_1} \right) \left(1 + \left[\frac{c}{c_2} \right]^{n_2} \right)} \quad (13)$$

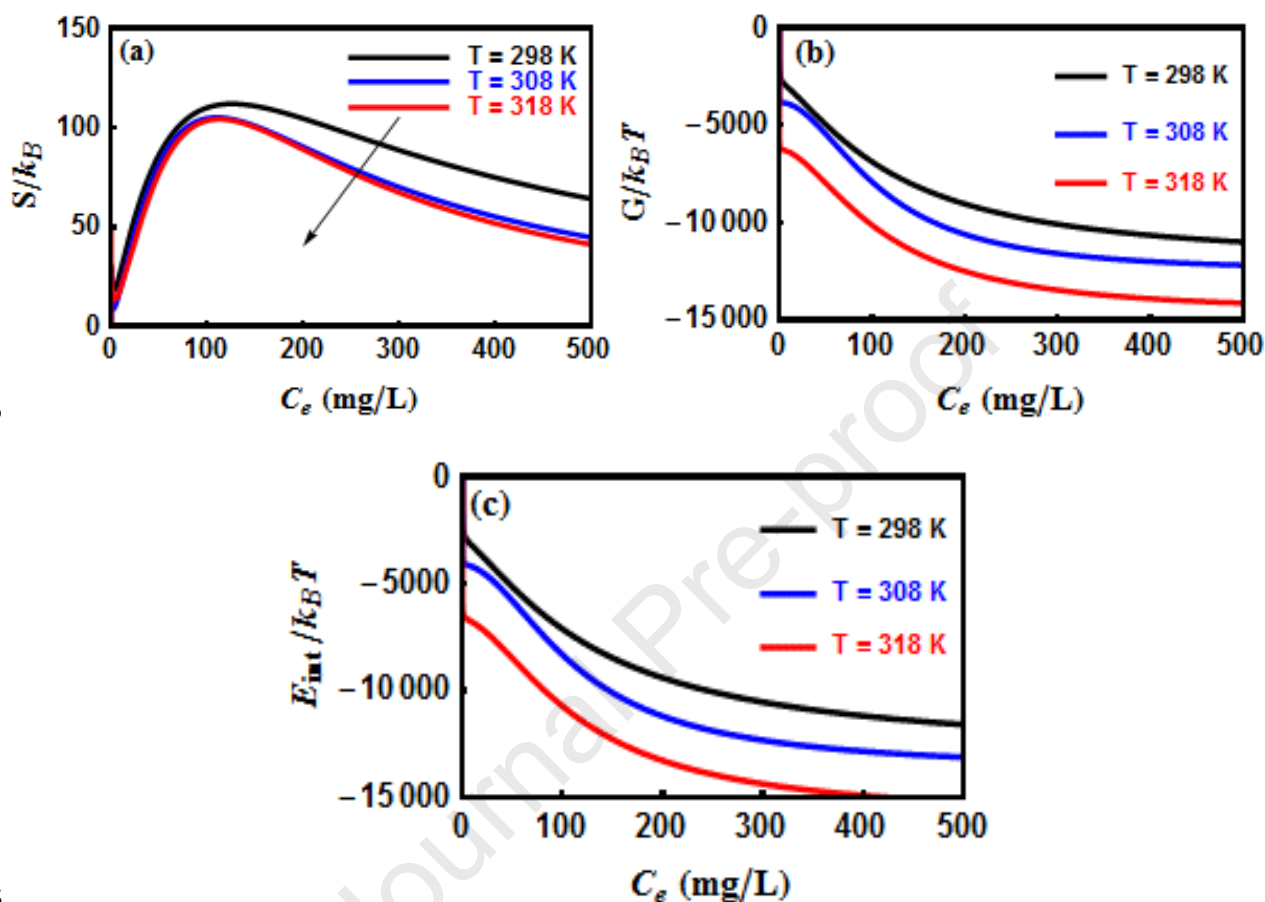
485 In Eqs. (11-13), k_B , μ and Z_{tr} are the Boltzmann constant, chemical potential and
 486 translation partition function, respectively.

487 The evolution of the entropy function during the OG dye adsorption versus equilibrium
 488 OG dye concentration at different temperatures (298, 308 and 318 K) is displayed in **Fig.**

489 **5(a)**. From this figure, the entropy function exhibited similar trend for all studied
490 temperatures. In addition, we can see that, with increasing the equilibrium OG dye
491 concentration, the entropy of OG dye removal system increased until a maximum at the
492 half-saturation concentration and then decreased. At lower OG dye concentrations, the
493 OG molecules possessed high probability to select an active site on the PANI@Fe-ZSM-5
494 surface, resulting in an increase of disorder at the solution-adsorbent interface. At higher
495 OG dye concentrations, the PANI@Fe-ZSM-5 surface tended to the saturation and the
496 probability of OG molecules to find a vacant adsorption site was significantly decreased.
497 Therefore, the entropy shifted towards lower values (decrease of disorder).

498 **Fig. 5(b)** represents the evolution of the free enthalpy as a function of OG dye
499 concentration. As a result, the negative values of the free enthalpy function revealed that
500 the OG adsorption on the PANI@Fe-ZSM-5 composite is a spontaneous process for all
501 investigated temperatures (Sellaoui et al., 2016). Besides, it can be seen that the free
502 enthalpy decreases with increasing temperature and OG dye concentration. Thus, we can
503 conclude that the OG dye adsorption process is more favorable at higher temperatures
504 (endothermic process) and higher OG dye concentrations (increase in the concentration
505 gradient). **Fig. 5(c)** displays the variation of internal energy versus equilibrium OG
506 concentration at different temperatures. The negative values of the internal energy during
507 the OG dye adsorption on the PANI@Fe-ZSM-5 composite confirms its spontaneous
508 nature (Sellaoui et al., 2017a), reflecting that the OG dye molecules exhibited good binding
509 affinity with the PANI@Fe-ZSM-5 surface. Moreover, the internal energy tremendously
510 decreases with OG concentration at low concentration range, which indicates that the OG
511 dye molecules target the most active sites on the PANI@Fe-ZSM-5 surface. When the OG
512 dye concentration is increased, the availability of PANI@Fe-ZSM-5 surface sites decreases

513 and the OG dye molecules interact with the less active sites, resulting in a slight
 514 diminution in the internal energy (Khalfaoui et al., 2015).



515

516

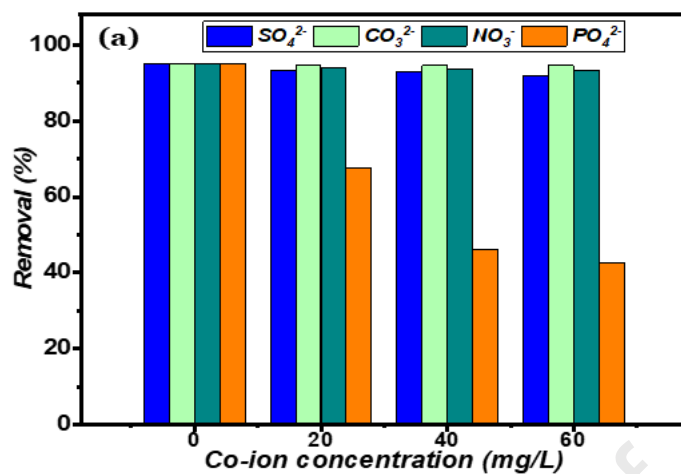
517 **Fig. 5.** Thermodynamic functions: **(a)** entropy; **(b)** free enthalpy and **(c)** internal
 518 energy for OG dye adsorption on the PANI@Fe-ZSM-5 composite.

519 3.6. Effect of co-existing ions and Regeneration

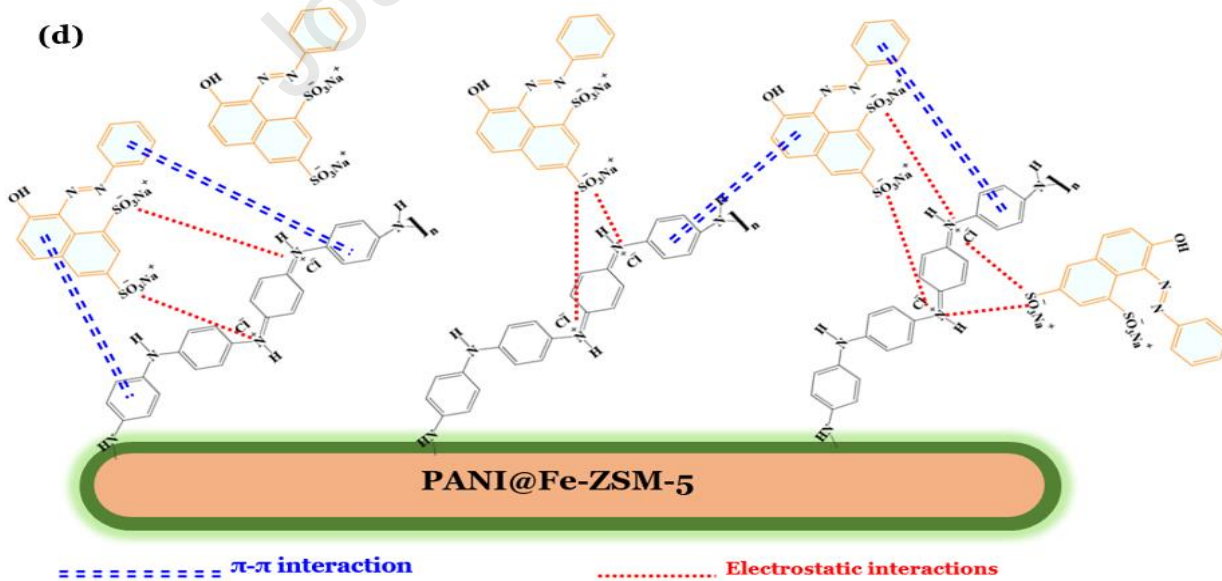
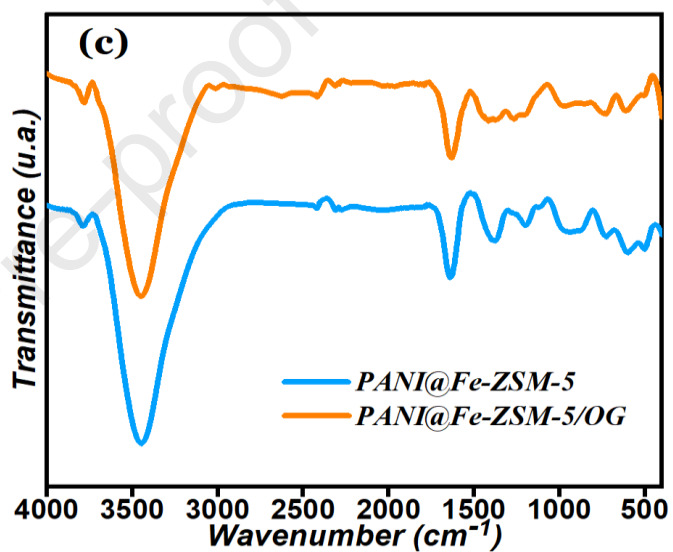
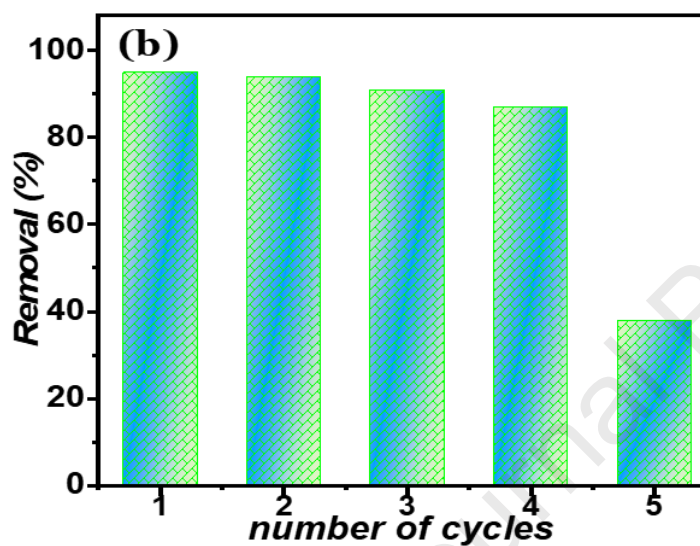
520 It has been known that the wastewaters are polluted not only by dyes, but also by other
 521 organic and inorganic pollutants (Ansari et al., 2017). Thus, it is necessary to assess the
 522 influence of coexisting ions. For this goal, a series of adsorption tests were carried out by
 523 keeping the concentration of OG dye constant at 20 mg/L while varying the concentration
 524 of coexisting ions (PO_4^{2-} , SO_4^{2-} , CO_3^{2-} and NO_3^-) from 20 to 60 mg/L. The operating

525 conditions were pH=6.0, adsorbent dose=0.5 g/L, contact time= 3 h and T = 25 °C. **Fig.**
526 **6(a)** shows the effect of coexisting ions on the performance of OG dye removal by
527 PANI@Fe-ZSM-5 composite (Laabd et al., 2021). The presence of SO_4^{2-} , CO_3^{2-} and NO_3^-
528 ions did not influence the OG removal and the adsorption capacity remained at 37.15
529 mg/g. In contrast, the presence of PO_4^{3-} ions had a considerable effect on the performance
530 of OG adsorption. The increase of concentration of PO_4^{2-} resulted in a decrease of the
531 amount of OG adsorbed until 17.03 mg/g. This adsorption behavior could be ascribed to
532 the affinity of PANI@Fe-ZSM-5 surface for PO_4^{3-} ions, and subsequently the competition
533 between OG dye and PO_4^{2-} anions significantly inhibited the OG adsorption (Banerjee et
534 al., 2019).

535 For regeneration and reuse of PANI@Fe-ZSM-5, NaOH (0.5 M) was used as a
536 regenerating agent. Further, it was reported in the literature that NaOH is the best suitable
537 agent for desorbing OG dye from the adsorbent surfaces (Brini et al., 2021a; Hsini et al.,
538 2021c; Xu et al., 2020). In this study, the recyclability of PANI@Fe-ZSM-5 composite for
539 OG dye removal efficiency was evaluated up to five adsorption-desorption cycles. **Fig.**
540 **6(b)** depicts that the adsorption efficiency of OG dye from aqueous solutions was still
541 above 86% in the first four desorption/adsorption cycles. However, in the fifth
542 regeneration cycle, the OG dye removal performance (38%) decreases significantly owing
543 to the possible accumulation of OG molecules on the PANI@Fe-ZSM-5 surface. Overall,
544 the experimental results revealed that the PANI@Fe-ZSM-5 composite owns excellent
545 reusability and could be reused as an efficient and inexpensive adsorbent to eliminate of
546 OG dye from aqueous solutions.



547



548

549 **Fig. 6. (a)** Effect of coexisting ions on the removal of OG dye by PANI@Fe-ZSM-5:
550 adsorbent dose = 0.5 g/L; pH= 6.0; 20 mg/L OG dye concentration; T=25°C; **(b)**
551 Adsorption efficiency of OG dye by PANI@Fe-ZSM-5 composite for 5 regeneration
552 cycles; **(c)** FT-IR spectral data of PANI@Fe-ZSM-5 before and after adsorption of OG
553 dye, and **(d)** Schematic **presentation** of the proposed adsorption mechanism.

554 **3.7. Comparison with other adsorbents**

555 To evaluate the adsorption performance of PANI@Fe-ZSM-5, it is important to figure out
556 its position compared with other adsorbents. From a literature survey, many studies
557 reported the OG dye adsorption from water using different adsorbent materials. As shown
558 in **Table 1**, it is evident that the PANI@Fe-ZSM-5 composite demonstrated an excellent
559 maximum uptake capacity (217 mg/g) for OG dye removal compared with reported
560 adsorbents. Thus, we conclude that the as-synthesized adsorbent may be a useful material
561 for efficient OG dye removal. Finally, the as-developed PANI@Fe-ZSM-5 hybrid material
562 can be recommended as a potential and inexpensive adsorbent to clean up OG dye from
563 wastewaters.

564 **Table 1.** Comparison of the maximum uptake capacities of PANI@Fe-ZSM-5 for OG
565 removal and other adsorbents addressed in the previously published studies.

566

567

568

Adsorbent	Q _{max} (mg g ⁻¹)	Operating conditions			Reference
		Equilibrium time (min)	Dose (g L ⁻¹)	pH	
FSMD MNPs	109.1	60	1	3	(Zheng et al., 2019)
Alumina nanoparticles	93.3	45	1	2.5	(Banerjee et al., 2019)
Cts(x)-g-PNVP	63.7	175	10	3	(Sutirman et al., 2019)
Monoamine-modified silica	36.3	300	1	3	(Donia et al., 2009)
Prussian-Blue nanoparticles supported over alumina	44.4	100	6.5	3	(Doumic et al., 2015)
AC from coffee grounds	100	180	1	3	(Laksaci et al., 2019)
Modified montmorillonite nanoclay	39.4	60	2.5	8	(Salam et al., 2017)
PANI@Walnut shells	17.24	90	1	6	(Imgharn et al., 2021)
Bagasse fly ash	18.79	200	2	4	(Mall et al., 2006)
Kapok fiber oriented polyaniline	192.3	240	1	6	(Zheng et al., 2012)
H-MIL -53(Fe)	163.9	300	--	4	(Feng et al., 2020)

PANI@AS biocomposite	190.98	100	0.5	5	(Hsini et al., 2020)
Cucumber peels	37.8	60	0.5	6	(Stavrinou et al., 2018)
PANI@Fe-ZSM-5 composite	217	120	0.5	5	Current study

569

570 **Conclusion**

571 In this contribution, PANI@Fe-ZSM-5 composite was synthesized, characterized and used
572 for OG dye removal from water. The adsorption study established that the PANI@Fe-
573 ZSM-5 composite as an effective adsorbent for the removal of OG dye from aqueous
574 solutions. Based on the results obtained for pH influence on the adsorption process and
575 PZC of PANI@Fe-ZSM-5 composite, electrostatic interactions were likely the main forces
576 governing the OG dye adsorption mechanism. The kinetic data for OG dye removal by the
577 PANI@Fe-ZSM-5 composite was well-fitted by the pseudo-second-order model. The mass
578 transfer process of OG dye from the solution to the PANI@Fe-ZSM-5 surface occurred via
579 three consecutive stages: (i) external diffusion, (ii) intraparticle diffusion and (iii) final
580 adsorption equilibrium. The OG dye binding mechanism and associated thermodynamic
581 behavior were evaluated on the basis of advanced statistical physics theory. Among the
582 fitted statistical physics models to the experimental findings, the **M3** model (monolayer
583 layer model with the different energy sites) is the best one to describe the OG dye
584 adsorption process. Based on this model, the macroscopic and microscopic aspects related
585 to the adsorption system were assessed. The OG dye molecules were adsorbed in the
586 perpendicular (multi-docking) and parallel (multimolecular) modes on the first ($n_1 < 1$)

587 and second ($n_2 > 1$) types of active sites in the PANI@Fe-ZSM-5 surface. The
 588 thermodynamic functions confirmed the feasibility of OG adsorption onto PANI@Fe-
 589 ZSM-5 composite through physical interactions. The theoretical data are in satisfactory
 590 concordance with experimental results. Finally, we can conclude that the as-developed
 591 PANI@Fe-ZSM-5 material can be applied as an efficient and regenerable adsorbent for
 592 treating the textile effluents.

593 **References**

- 594 Abbasi, M., 2017. Synthesis and characterization of magnetic nanocomposite of
 595 chitosan/SiO₂/carbon nanotubes and its application for dyes removal. *J. Clean.*
 596 *Prod.* 145, 105–113. <https://doi.org/10.1016/j.jclepro.2017.01.046>
 597 Abdel Hamid, Z., Hasan Gomaa, M., S. Abdel Rehim, S., Abdel Hamid, M., Ibrahim, A.,
 598 2019. Synthesis and Characterization of Nanostructured Polyaniline Thin Films
 599 with Superhydrophobic Properties. *Coatings* 9, 748.
 600 <https://doi.org/10.3390/coatings9110748>
 601 Abdellaoui, Y., Gamero-Melo, P., Díaz-Jiménez, L., Ponce-Caballero, C., Giacomani-
 602 Vallejos, G., 2020. Synthesis and Surface Modification of Small Pore Size Zeolite
 603 W for Improving Removal Efficiency of Anionic Contaminants from Water. *Bull.*
 604 *Environ. Contam. Toxicol.* 105, 934–940. [https://doi.org/10.1007/s00128-020-](https://doi.org/10.1007/s00128-020-03036-z)
 605 [03036-z](https://doi.org/10.1007/s00128-020-03036-z)
 606 Ait Haki, M., Imgharn, A., Aarab, N., Hsini, A., Essekre, A., Laabd, M., El Jazouli, H.,
 607 Elamine, M., Lakhmiri, R., Albourine, A., 2021. Efficient removal of crystal violet
 608 dye from aqueous solutions using sodium hydroxide modified avocado shells:
 609 kinetics and isotherms modeling. *Water Sci. Technol.* **wst2021451**.
 610 <https://doi.org/10.2166/wst.2021.451>
 611 Akhsassi, B., Bouddouch, A., Naciri, Y., Bakiz, B., Taoufyq, A., Favotto, C., Villain, S.,
 612 Guinneton, F., Benlhachemi, A., 2021. Enhanced photocatalytic activity of
 613 Zn₃(PO₄)₂/ZnO composite semiconductor prepared by different methods. *Chem.*
 614 *Phys. Lett.* 783, 139046. <https://doi.org/10.1016/j.cplett.2021.139046>
 615 Amjlef, A., Khrach, S., Ait El Fakir, A., Farsad, S., Et-Taleb, S., El Alem, N., 2021.
 616 Adsorptive properties investigation of natural sand as adsorbent for methylene
 617 blue removal from contaminated water. *Nanotechnol. Environ. Eng.* 6, 26.
 618 <https://doi.org/10.1007/s41204-021-00119-y>
 619 Ansari, M.O., Kumar, R., Ansari, S.A., Ansari, S.P., Barakat, M.A., Alshahrie, A., Cho,
 620 M.H., 2017. Anion selective pTSA doped polyaniline@graphene oxide-
 621 multiwalled carbon nanotube composite for Cr(VI) and Congo red adsorption. *J.*
 622 *Colloid Interface Sci.* 496, 407–415. <https://doi.org/10.1016/j.jcis.2017.02.034>
 623 Ayachi, F., Z. Kyzas, G., Aatrous, M., Sakly, A., Ben Lamine, A., 2019. Evaluating the
 624 adsorption of Ni(II) and Cu(II) on spirulina biomass by statistical physics

- 625 formalism. *J. Ind. Eng. Chem.* 80, 461–470.
626 <https://doi.org/10.1016/j.jiec.2019.05.044>
- 627 Ba Mohammed, B., Hsini, A., Abdellaoui, Y., Abou Oualid, H., Laabd, M., El Ouardi, M.,
628 Ait Addi, A., Yamni, K., Tijani, N., 2020. Fe-ZSM-5 zeolite for efficient removal of
629 basic Fuchsin dye from aqueous solutions: Synthesis, characterization and
630 adsorption process optimization using BBD-RSM modeling. *J. Environ. Chem.*
631 *Eng.* 8, 104419. <https://doi.org/10.1016/j.jece.2020.104419>
- 632 Banerjee, S., Dubey, S., Gautam, R.K., Chattopadhyaya, M.C., Sharma, Y.C., 2019.
633 Adsorption characteristics of alumina nanoparticles for the removal of hazardous
634 dye, Orange G from aqueous solutions. *Arab. J. Chem.* 12, 5339–5354.
635 <https://doi.org/10.1016/j.arabjc.2016.12.016>
- 636 Belbachir, I., Makhoukhi, B., 2017. Adsorption of Bezathren dyes onto sodic bentonite
637 from aqueous solutions. *J. Taiwan Inst. Chem. Eng.* 75, 105–111.
638 <https://doi.org/10.1016/j.jtice.2016.09.042>
- 639 Benjelloun, M., Miyah, Y., Akdemir Evrendilek, G., Zerrouq, F., Lairini, S., 2021. Recent
640 Advances in Adsorption Kinetic Models: Their Application to Dye Types. *Arab. J.*
641 *Chem.* 14, 103031. <https://doi.org/10.1016/j.arabjc.2021.103031>
- 642 Bhaumik, M., Maity, A., Brink, H.G., 2021. Zero valent nickel nanoparticles decorated
643 polyaniline nanotubes for the efficient removal of Pb(II) from aqueous solution:
644 Synthesis, characterization and mechanism investigation. *Chem. Eng. J.* 417,
645 127910. <https://doi.org/10.1016/j.cej.2020.127910>
- 646 Brini, L., H'Maida, K., Imgharn, A., Hsini, A., Naciri, Y., Ajmal, Z., Bouziani, A.,
647 Boulahya, A., Arahou, M., Bakiz, B., Albourine, A., Fekhaoui, M., 2021a. Synthesis
648 and characterisation of PANI- coated Heliotrope Leaves (PANI@HL) with high
649 clean-up capacity for Orange G dye from aqueous media. *Int. J. Environ. Anal.*
650 *Chem.* 1–17. <https://doi.org/10.1080/03067319.2021.1994557>
- 651 Brini, L., Hsini, A., Naciri, Y., Bouziani, A., Ajmal, Z., H'Maida, K., Boulahya, A., Arahou,
652 M., Bakiz, B., Albourine, A., Fekhaoui, M., 2021b. Synthesis and characterization
653 of arginine-doped heliotrope leaves with high clean-up capacity for crystal violet
654 dye from aqueous media. *Water Sci. Technol.* 84, 2265–2277.
655 <https://doi.org/10.2166/wst.2021.446>
- 656 Chan, H.S.O., Ng, S.C., Sim, W.S., Tan, K.L., Tan, B.T.G., 1992. Preparation and
657 characterization of electrically conducting copolymers of aniline and anthranilic
658 acid: evidence for self-doping by x-ray photoelectron spectroscopy.
659 *Macromolecules* 25, 6029–6034. <https://doi.org/10.1021/ma00048a026>
- 660 Donia, A.M., Atia, A.A., Al-amrani, W.A., El-Nahas, A.M., 2009. Effect of structural
661 properties of acid dyes on their adsorption behaviour from aqueous solutions by
662 amine modified silica. *J. Hazard. Mater.* 161, 1544–1550.
663 <https://doi.org/10.1016/j.jhazmat.2008.05.042>
- 664 Doula, M.K., 2007. Synthesis of a clinoptilolite–Fe system with high Cu sorption
665 capacity. *Chemosphere* 67, 731–740.
666 <https://doi.org/10.1016/j.chemosphere.2006.10.072>
- 667 Doumic, L., Salierno, G., Cassanello, M., Haure, P., Ayude, M., 2015. Efficient removal of
668 Orange G using Prussian Blue nanoparticles supported over alumina. *Catal.*
669 *Today* 240, 67–72. <https://doi.org/10.1016/j.cattod.2014.03.064>
- 670 Fahoul, Y., Tanji, K., Zouheir, M., Mrabet, I.E., Naciri, Y., Hsini, A., Nahali, L.,
671 Kherbeche, A., 2022. Novel River Sediment@ZnO Co nanocomposite for

- 672 photocatalytic degradation and COD reduction of crystal violet under visible light.
673 *J. Mol. Struct.* 1253, 132298. <https://doi.org/10.1016/j.molstruc.2021.132298>
- 674 Feng, T., Bavumiragira, J.P., Wambui, M.A., Kabtamu, D.M., László, K., Wang, Y., Li, F.,
675 2020. Hierarchical porous induced competent removal of low concentration azo
676 dye molecules by generating a leachy crystalline structure H-MIL-53(Fe). *Chin.*
677 *Chem. Lett.* 31, 2717–2720. <https://doi.org/10.1016/j.ccllet.2020.04.044>
- 678 Fiol, N., Villaescusa, I., 2009. Determination of sorbent point zero charge: usefulness in
679 sorption studies. *Environ. Chem. Lett.* 7, 79–84. [https://doi.org/10.1007/s10311-](https://doi.org/10.1007/s10311-008-0139-0)
680 [008-0139-0](https://doi.org/10.1007/s10311-008-0139-0)
- 681 Gottlieb, A., Shaw, C., Smith, A., Wheatley, A., Forsythe, S., 2003. The toxicity of textile
682 reactive azo dyes after hydrolysis and decolourisation. *J. Biotechnol.* 101, 49–56.
683 [https://doi.org/10.1016/S0168-1656\(02\)00302-4](https://doi.org/10.1016/S0168-1656(02)00302-4)
- 684 Hassan, M.M., Carr, C.M., 2018. A critical review on recent advancements of the removal
685 of reactive dyes from dyehouse effluent by ion-exchange adsorbents.
686 *Chemosphere* 209, 201–219.
687 <https://doi.org/10.1016/j.chemosphere.2018.06.043>
- 688 Hsini, A., Benafqir, M., Naciri, Y., Laabd, M., Bouziani, A., Ez-zahery, M., Lakhmiri, R.,
689 Alem, N.E., Albourine, A., 2021a. Synthesis of an arginine-functionalized
690 polyaniline@FeOOH composite with high removal performance of hexavalent
691 chromium ions from water: Adsorption behavior, regeneration and process
692 capability studies. *Colloids Surf. Physicochem. Eng. Asp.* 617, 126274.
693 <https://doi.org/10.1016/j.colsurfa.2021.126274>
- 694 Hsini, A., Essekre, A., Aarab, N., Laabd, M., Ait Addi, A., Lakhmiri, R., Albourine, A.,
695 2020. Elaboration of novel polyaniline@Almond shell biocomposite for effective
696 removal of hexavalent chromium ions and Orange G dye from aqueous solutions.
697 *Environ. Sci. Pollut. Res.* 27, 15245–15258. [https://doi.org/10.1007/s11356-020-](https://doi.org/10.1007/s11356-020-08039-1)
698 [08039-1](https://doi.org/10.1007/s11356-020-08039-1)
- 699 Hsini, A., Naciri, Y., Benafqir, M., Ajmal, Z., Aarab, N., Laabd, M., Navío, J.A., Puga, F.,
700 Boukherroub, R., Bakiz, B., Albourine, A., 2021b. Facile synthesis and
701 characterization of a novel 1,2,4,5-benzene tetracarboxylic acid doped
702 polyaniline@zinc phosphate nanocomposite for highly efficient removal of
703 hazardous hexavalent chromium ions from water. *J. Colloid Interface Sci.* 585,
704 560–573. <https://doi.org/10.1016/j.jcis.2020.10.036>
- 705 Hsini, A., Naciri, Y., Bouziani, A., Aarab, N., Essekre, A., Imgharn, A., Laabd, M., Navío,
706 J.A., Puga, F., Lakhmiri, R., Albourine, A., 2021c. Polyaniline coated tungsten
707 trioxide as an effective adsorbent for the removal of orange G dye from aqueous
708 media. *RSC Adv.* 11, 31272–31283. <https://doi.org/10.1039/D1RA04135E>
- 709 Hsini, A., Naciri, Y., Laabd, M., Bouziani, A., Navío, J.A., Puga, F., Boukherroub, R.,
710 Lakhmiri, R., Albourine, A., 2021d. Development of a novel PANI@WO₃ hybrid
711 composite and its application as a promising adsorbent for Cr(VI) ions removal. *J.*
712 *Environ. Chem. Eng.* 9, 105885. <https://doi.org/10.1016/j.jece.2021.105885>
- 713 Imgharn, A., ighnih, H., Hsini, A., Naciri, Y., Laabd, M., Kabli, H., Elamine, M.,
714 Lakhmiri, R., Souhail, B., Albourine, A., 2021. Synthesis and characterization of
715 polyaniline-based biocomposites and their application for effective removal of
716 Orange G dye using Adsorption in dynamic regime. *Chem. Phys. Lett.* 138811.
717 <https://doi.org/10.1016/j.cplett.2021.138811>

- 718 Kachangoon, R., Vichapong, J., Santaladchaiyakit, Y., Burakham, R., Srijaranai, S.,
719 2020. An Eco-Friendly Hydrophobic Deep Eutectic Solvent-Based Dispersive
720 Liquid-Liquid Microextraction for the Determination of Neonicotinoid
721 Insecticide Residues in Water, Soil and Egg Yolk Samples. *Molecules* 25, 2785.
722 <https://doi.org/10.3390/molecules25122785>
- 723 Khalfaoui, M., Ghali, A.E., Aguir, C., Mohamed, Z., Baouab, M.H.V., Lamine, A.B., 2015.
724 Study on adsorption of herbicide onto functionalized cellulose extracted from
725 *Juncus acutus* L. plant: Experimental results and theoretical modeling. *Ind. Crops*
726 *Prod.* 67, 169–178. <https://doi.org/10.1016/j.indcrop.2015.01.032>
- 727 Kumar, P.A., Chakraborty, S., Ray, M., 2008. Removal and recovery of chromium from
728 wastewater using short chain polyaniline synthesized on jute fiber. *Chem. Eng. J.*
729 141, 130–140. <https://doi.org/10.1016/j.cej.2007.11.004>
- 730 Laabd, M., Brahmi, Y., El Ibrahimy, B., Hsini, A., Toufik, E., Abdellaoui, Y., Abou Oualid,
731 H., El Ouardi, M., Albourine, A., 2021. A novel mesoporous
732 Hydroxyapatite@Montmorillonite hybrid composite for high-performance
733 removal of emerging Ciprofloxacin antibiotic from water: Integrated experimental
734 and Monte Carlo computational assessment. *J. Mol. Liq.* 338, 116705.
735 <https://doi.org/10.1016/j.molliq.2021.116705>
- 736 Laabd, M., Chafai, H., Esseki, A., Elamine, M., Al-Muhtaseb, S.A., Lakhmiri, R.,
737 Albourine, A., 2017. Single and multi-component adsorption of aromatic acids
738 using an eco-friendly polyaniline-based biocomposite. *Sustain. Mater. Technol.*
739 12, 35–43. <https://doi.org/10.1016/j.susmat.2017.04.004>
- 740 Laabd, M., Imgharn, A., Hsini, A., Naciri, Y., Mobarak, M., Szunerits, S., Boukherroub,
741 R., Albourine, A., 2022. Efficient detoxification of Cr(VI)-containing effluents by
742 sequential adsorption and reduction using a novel cysteine-doped
743 PANi@faujasite composite: Experimental study supported by advanced statistical
744 physics prediction. *J. Hazard. Mater.* 422, 126857.
745 <https://doi.org/10.1016/j.jhazmat.2021.126857>
- 746 Laksaci, H., Khelifi, A., Belhamdi, B., Trari, M., 2019. The use of prepared activated
747 carbon as adsorbent for the removal of orange G from aqueous solution.
748 *Microchem. J.* 145, 908–913. <https://doi.org/10.1016/j.microc.2018.12.001>
- 749 Li, Z., Sellaoui, L., Dotto, G.L., Lamine, A.B., Bonilla-Petriciolet, A., Hanafy, H.,
750 Belmabrouk, H., Netto, M.S., Erto, A., 2019. Interpretation of the adsorption
751 mechanism of Reactive Black 5 and Ponceau 4R dyes on chitosan/polyamide
752 nanofibers via advanced statistical physics model. *J. Mol. Liq.* 285, 165–170.
753 <https://doi.org/10.1016/j.molliq.2019.04.091>
- 754 Liao, G., Li, Q., Xu, Z., 2019. The chemical modification of polyaniline with enhanced
755 properties: A review. *Prog. Org. Coat.* 126, 35–43.
756 <https://doi.org/10.1016/j.porgcoat.2018.10.018>
- 757 Liu, G., Xiangli, F., Wei, W., Liu, S., Jin, W., 2011. Improved performance of
758 PDMS/ceramic composite pervaporation membranes by ZSM-5 homogeneously
759 dispersed in PDMS via a surface graft/coating approach. *Chem. Eng. J.* 174, 495–
760 503. <https://doi.org/10.1016/j.cej.2011.06.004>
- 761 Mall, I.D., Srivastava, V.C., Agarwal, N.K., 2006. Removal of Orange-G and Methyl
762 Violet dyes by adsorption onto bagasse fly ash—kinetic study and equilibrium
763 isotherm analyses. *Dyes Pigments* 69, 210–223.
764 <https://doi.org/10.1016/j.dyepig.2005.03.013>

- 765 Mimouni, I., Bouziani, A., Naciri, Y., Boujnah, M., El Belghiti, M.A., El Azzouzi, M.,
766 2021. Effect of heat treatment on the photocatalytic activity of α -Fe₂O₃
767 nanoparticles: towards diclofenac elimination. *Environ. Sci. Pollut. Res.*
768 <https://doi.org/10.1007/s11356-021-16146-w>
- 769 Mobarak, M., Mohamed, E.A., Selim, A.Q., Eissa, M.F., Seliem, M.K., 2019a.
770 Experimental results and theoretical statistical modeling of malachite green
771 adsorption onto MCM-41 silica/rice husk composite modified by beta radiation.
772 *J. Mol. Liq.* 273, 68–82. <https://doi.org/10.1016/j.molliq.2018.09.132>
- 773 Mobarak, M., Mohamed, E.A., Selim, A.Q., Mohamed, F.M., Sellaoui, L., Bonilla-
774 Petriciolet, A., Seliem, M.K., 2019b. Statistical physics modeling and
775 interpretation of methyl orange adsorption on high-order mesoporous composite
776 of MCM-48 silica with treated rice husk. *J. Mol. Liq.* 285, 678–687.
777 <https://doi.org/10.1016/j.molliq.2019.04.116>
- 778 Mohamed, E.A., Mobarak, M., Kumar, R., Barakat, M.A., Bonilla-Petriciolet, A., Seliem,
779 M.K., Selim, A.Q., 2020. Novel hybrid multifunctional composite of chitosan and
780 altered basalt for barium adsorption: Experimental and theoretical studies.
781 *Colloids Surf. Physicochem. Eng. Asp.* 593, 124613.
782 <https://doi.org/10.1016/j.colsurfa.2020.124613>
- 783 Naciri, Y., Hsini, A., Bouziani, A., Djellabi, R., Ajmal, Z., Laabd, M., Navío, J.A., Mills, A.,
784 Bianchi, C.L., Li, H., Bakiz, B., Albourine, A., 2021. Photocatalytic oxidation of
785 pollutants in gas-phase via Ag₃PO₄-based semiconductor photocatalysts: Recent
786 progress, new trends, and future perspectives. *Crit. Rev. Environ. Sci. Technol.* 1–
787 44. <https://doi.org/10.1080/10643389.2021.1877977>
- 788 Naciri, Y., Hsini, A., Bouziani, A., Tanji, K., El Ibrahimy, B., Ghazzal, M.N., Bakiz, B.,
789 Albourine, A., Benlhachemi, A., Navío, J.A., Li, H., 2022. Z-scheme WO₃/PANI
790 heterojunctions with enhanced photocatalytic activity under visible light: A depth
791 experimental and DFT studies. *Chemosphere* 292, 133468.
792 <https://doi.org/10.1016/j.chemosphere.2021.133468>
- 793 Narayanan, S., Vijaya, J.J., Sivasanker, S., Kennedy, L.J., Jesudoss, S.K., 2015.
794 Structural, morphological and catalytic investigations on hierarchical ZSM-5
795 zeolite hexagonal cubes by surfactant assisted hydrothermal method. *Powder*
796 *Technol.* 274, 338–348. <https://doi.org/10.1016/j.powtec.2015.01.054>
- 797 Nasar, A., Mashkour, F., 2019. Application of polyaniline-based adsorbents for dye
798 removal from water and wastewater—a review. *Environ. Sci. Pollut. Res.* 26,
799 5333–5356. <https://doi.org/10.1007/s11356-018-3990-y>
- 800 Niu, X.R., Li, J., Zhang, L., Lei, Z.T., Zhao, X.L., Yang, C.H., 2017. ZSM-5 functionalized
801 in situ with manganese ions for the catalytic oxidation of cyclohexane. *RSC Adv* 7,
802 50619–50625. <https://doi.org/10.1039/C7RA10771D>
- 803 Njoya, O., Zhao, S., Qu, Y., Shen, J., Wang, B., Shi, H., Chen, Z., 2020. Performance and
804 potential mechanism of Cr(VI) reduction and subsequent Cr(III) precipitation
805 using sodium borohydride driven by oxalate. *J. Environ. Manage.* 275, 111165.
806 <https://doi.org/10.1016/j.jenvman.2020.111165>
- 807 Ravelo-Acuña, D., Fuentes-García, J.A., Yee-Madeira, H.T., Diaz-Cano, A.I., Goya, G.F.,
808 Santoyo-Salazar, J., 2019. Sonochemical magnetite encapsulation in silica at low
809 irradiation power. *Mater. Lett.* 250, 103–107.
810 <https://doi.org/10.1016/j.matlet.2019.04.073>

- 811 Renault, F., Sancey, B., Badot, P.-M., Crini, G., 2009. Chitosan for
812 coagulation/flocculation processes – An eco-friendly approach. *Eur. Polym. J.* 45,
813 1337–1348. <https://doi.org/10.1016/j.eurpolymj.2008.12.027>
- 814 Sahu, S., Sahu, U.K., Patel, R.K., 2019. Modified Thorium Oxide Polyaniline Core–Shell
815 Nanocomposite and Its Application for the Efficient Removal of Cr(VI). *J. Chem.*
816 *Eng. Data* 64, 1294–1304. <https://doi.org/10.1021/acs.jced.8b01225>
- 817 Saifuddin, M., Bae, J., Kim, K.S., 2019. Role of Fe, Na and Al in Fe-Zeolite-A for
818 adsorption and desorption of phosphate from aqueous solution. *Water Res.* 158,
819 246–256. <https://doi.org/10.1016/j.watres.2019.03.045>
- 820 Salam, M.A., Kosa, S.A., Al-Beladi, A.A., 2017. Application of nanoclay for the adsorptive
821 removal of Orange G dye from aqueous solution. *J. Mol. Liq.* 241, 469–477.
822 <https://doi.org/10.1016/j.molliq.2017.06.055>
- 823 Seliem, M.K., Mobarak, M., 2019. Cr(VI) uptake by a new adsorbent of CTAB–modified
824 carbonized coal: Experimental and advanced statistical physics studies. *J. Mol.*
825 *Liq.* 294, 111676. <https://doi.org/10.1016/j.molliq.2019.111676>
- 826 Sellaoui, L., Depci, T., Kul, A.R., Knani, S., Ben Lamine, A., 2016. A new statistical
827 physics model to interpret the binary adsorption isotherms of lead and zinc on
828 activated carbon. *J. Mol. Liq.* 214, 220–230.
829 <https://doi.org/10.1016/j.molliq.2015.12.080>
- 830 Sellaoui, L., Dotto, G.L., Wjihi, S., Gonçalves, J.O., Pinto, L.A.A., Lamine, A.B., Erto, A.,
831 2017a. Thermodynamic analysis of single and binary adsorption of Food Yellow 4
832 and Food Blue 2 on CC-chitosan: Application of statistical physics and IAST
833 models. *J. Mol. Liq.* 232, 499–505. <https://doi.org/10.1016/j.molliq.2017.02.103>
- 834 Sellaoui, L., Guedidi, H., Knani, S., Reinert, L., Duclaux, L., Ben Lamine, A., 2015.
835 Application of statistical physics formalism to the modeling of adsorption
836 isotherms of ibuprofen on activated carbon. *Fluid Phase Equilibria* 387, 103–110.
837 <https://doi.org/10.1016/j.fluid.2014.12.018>
- 838 Sellaoui, L., Mechi, N., Lima, É.C., Dotto, G.L., Ben Lamine, A., 2017b. Adsorption of
839 diclofenac and nimesulide on activated carbon: Statistical physics modeling and
840 effect of adsorbate size. *J. Phys. Chem. Solids* 109, 117–123.
841 <https://doi.org/10.1016/j.jpcs.2017.05.019>
- 842 Shyaa, A.A., Hasan, O.A., Abbas, A.M., 2015. Synthesis and characterization of
843 polyaniline/zeolite nanocomposite for the removal of chromium(VI) from
844 aqueous solution. *J. Saudi Chem. Soc.* 19, 101–107.
845 <https://doi.org/10.1016/j.jscs.2012.01.001>
- 846 Stavrinou, A., Aggelopoulos, C.A., Tsakiroglou, C.D., 2018. Exploring the adsorption
847 mechanisms of cationic and anionic dyes onto agricultural waste peels of banana,
848 cucumber and potato: Adsorption kinetics and equilibrium isotherms as a tool. *J.*
849 *Environ. Chem. Eng.* 6, 6958–6970. <https://doi.org/10.1016/j.jece.2018.10.063>
- 850 Suresh, R., Giribabu, K., Manigandan, R., Stephen, A., Narayanan, V., 2014. Fabrication
851 of Ni–Fe₂O₃ magnetic nanorods and application to the detection of uric acid.
852 *RSC Adv.* 4, 17146. <https://doi.org/10.1039/c4ra00725e>
- 853 Sutirman, Z.A., Sanagi, M.M., Abd Karim, K.J., Abu Naim, A., Wan Ibrahim, W.A., 2019.
854 Enhanced removal of Orange G from aqueous solutions by modified chitosan
855 beads: Performance and mechanism. *Int. J. Biol. Macromol.* 133, 1260–1267.
856 <https://doi.org/10.1016/j.ijbiomac.2019.04.188>

- 857 Tang, D., Zhang, G., 2016. Efficient removal of fluoride by hierarchical Ce–Fe bimetal
858 oxides adsorbent: Thermodynamics, kinetics and mechanism. *Chem. Eng. J.* 283,
859 721–729. <https://doi.org/10.1016/j.cej.2015.08.019>
- 860 Tu, B., Wen, R., Wang, K., Cheng, Y., Deng, Y., Cao, W., Zhang, K., Tao, H., 2020.
861 Efficient removal of aqueous hexavalent chromium by activated carbon derived
862 from Bermuda grass. *J. Colloid Interface Sci.* 560, 649–658.
863 <https://doi.org/10.1016/j.jcis.2019.10.103>
- 864 Wang, Q., Qiu, S., Wang, S., Shang, J., Zhao, R., Wu, X., Chen, W., Zhou, H., Wang, X.,
865 2015. Graphene oxide/polyaniline nanotube composites synthesized in alkaline
866 aqueous solution. *Synth. Met.* 210, 314–322.
867 <https://doi.org/10.1016/j.synthmet.2015.10.017>
- 868 Wang, X., Liu, N., Yan, X., Zhang, W., Wei, Y., 2005. Alkali-guided Synthesis of
869 Polyaniline Hollow Microspheres. *Chem. Lett.* 34, 42–43.
870 <https://doi.org/10.1246/cl.2005.42>
- 871 Wjihi, S., Aouaini, F., Almuqrin, A.H., Lamine, A.B., 2020. Physicochemical assessment
872 of prednisone adsorption on two molecular composites using statistical physics
873 formalism in cosmetics. *Arab. J. Chem.* 13, 6876–6886.
874 <https://doi.org/10.1016/j.arabjc.2020.06.040>
- 875 Wjihi, S., Sellaoui, L., Bouzid, M., Dhaou, H., Knani, S., Jemni, A., Ben Lamine, A., 2017.
876 Theoretical study of hydrogen sorption on LaNi₅ using statistical physics
877 treatment: microscopic and macroscopic investigation. *Int. J. Hydrog. Energy* 42,
878 2699–2712. <https://doi.org/10.1016/j.ijhydene.2016.10.102>
- 879 Xu, H., Zhang, J., Chen, Y., Lu, H., Zhuang, J., Li, J., 2014. Synthesis of polyaniline-
880 modified MnO₂ composite nanorods and their photocatalytic application. *Mater.*
881 *Lett.* 117, 21–23. <https://doi.org/10.1016/j.matlet.2013.11.089>
- 882 Xu, M.-Y., Jiang, H.-L., Xie, Z.-W., Li, Z.-T., Xu, D., He, F.-A., 2020. Highly efficient
883 selective adsorption of anionic dyes by modified β -cyclodextrin polymers. *J.*
884 *Taiwan Inst. Chem. Eng.* 108, 114–128.
885 <https://doi.org/10.1016/j.jtice.2020.01.005>
- 886 Yeamin, Md.B., Islam, Md.M., Chowdhury, A.-N., Awual, Md.R., 2021. Efficient
887 encapsulation of toxic dyes from wastewater using several biodegradable natural
888 polymers and their composites. *J. Clean. Prod.* 291, 125920.
889 <https://doi.org/10.1016/j.jclepro.2021.125920>
- 890 Zhang, J., Gao, J., Song, Q., Guo, Z., Chen, A., Chen, G., Zhou, S., 2016. N-substituted
891 Carboxyl Polyaniline Covalent Grafting Reduced Graphene Oxide
892 Nanocomposites and Its Application in Supercapacitor. *Electrochimica Acta* 199,
893 70–79. <https://doi.org/10.1016/j.electacta.2016.03.003>
- 894 Zheng, X., Zheng, H., Zhou, Y., Sun, Y., Zhao, R., Liu, Y., Zhang, S., 2019. Enhanced
895 adsorption of Orange G from aqueous solutions by quaternary ammonium group-
896 rich magnetic nanoparticles. *Colloids Surf. Physicochem. Eng. Asp.* 580, 123746.
897 <https://doi.org/10.1016/j.colsurfa.2019.123746>
- 898 Zheng, Y., Liu, Y., Wang, A., 2012. Kapok Fiber Oriented Polyaniline for Removal of
899 Sulfonated Dyes. *Ind. Eng. Chem. Res.* 51, 10079–10087.
900 <https://doi.org/10.1021/ie300246m>
- 901 Zhou, T., Li, C., Jin, H., Lian, Y., Han, W., 2017. Effective Adsorption/Reduction of
902 Cr(VI) Oxyanion by Halloysite@Polyaniline Hybrid Nanotubes. *ACS Appl. Mater.*
903 *Interfaces* 9, 6030–6043. <https://doi.org/10.1021/acsami.6b14079>

Journal Pre-proof

Highlights

- ✓ A novel PANI@Fe-ZSM-5 hybrid composite was easily elaborated and fully characterized.
- ✓ The adsorption performance of PANI@Fe-ZSM-5 towards OG dye was investigated.
- ✓ The OG dye binding mechanism was assessed by advanced statistical physics modeling.
- ✓ Statistical physics parameters and thermodynamic functions of the adsorption system were studied.
- ✓ PANI@Fe-ZSM-5 composite has excellent adsorption ability and satisfactory reusability.

Declaration of Interest Statement

- The authors declare that they have no known competing financial interests or personal relationships that could have appeared to influence the work reported in this paper.

Journal Pre-proof